

Multibody Structural Analysis and Design Improvements of Dynamically Running Linear Vibrating Feeders

Efekan ŞENCAN ^a, Yakup Taner TAŞDELEN ^a, Özge Güler ^b, Paşa YAYLA ^{a*}

a. *Marmara University, Engineering Faculty, Mechanical Engineering Department, Istanbul, 34840, Türkiye*

b. *R&D Center, Burçelik Bursa Çelik Döküm Sanayi A.Ş., Bursa, 16159, Türkiye*

*Correspondence author: paşa.yayla@marmara.edu.tr (Paşa YAYLA)

Keywords	Abstract
Vibrating feeder; Multi-body dynamics; Dynamic structural analysis; Design improvements; FEA	<p>Vibrating feeders play a crucial role in various industries by ensuring the efficient transfer of materials and ensuring optimum material flow rates through effective operation. This study investigates the stress variations in a specific vibrating feeder during static and dynamic phases. It determines the cause of damage to a feeder that has previously been damaged and proposes solutions to prevent future damage through minor design modifications. The loads on the feeder were analyzed in detail using ANSYS software, and the finite element method was used to identify the fatigue zones. The results of the static, modal, transient structural, and fatigue analyses indicate that fatigue-related stresses and incorrect operating frequencies may lead to the feeder's fracture. This analysis provides valuable information to strengthen the design and prevent future failures.</p> <p>This study uniquely integrates multi-body dynamics analysis to examine the dynamic interactions between feeder components, offering enhanced predictive capabilities for operational performance. The findings emphasize the importance of iterative design processes and advanced analytical techniques in developing robust and durable mechanical systems. Future research directions include exploring alternative materials, optimizing vibro motor configurations, investigating resonance control strategies, and incorporating energy-efficient designs and real-time monitoring to further enhance feeder performance in diverse industrial applications.</p>

Highlights

- The manuscript uses a multi-body-dynamic approach to investigate the failure of a vibrating feeder and the design improvements with the help of finite element analysis.
- This study uniquely integrates static, modal, transient, fatigue, and multi-body dynamics analysis to provide a comprehensive view of feeder performance—an area not extensively covered in the existing literature.
- The study demonstrates the effectiveness of the design improvements, highlighting the importance of thorough analysis and iterative design in improving the performance and durability of mechanical components.

1. Introduction

In industrial and mining operations, vibrating feeders play a crucial role in material processing by delivering materials to processes or machines via vibration [1]. These systems consist of a vibratory drive unit, a vibrating feeder bowl, an amplitude controller, and an inline feeder and track [2]. However, excessive vibration can lead to malfunctions, reducing performance and reliability. Significant potential challenges are faced by vibrating feeders, with controlling excessive vibration being paramount, as it can lead to infrequent failures, reduced material flow accuracy, and mechanical damage. This not only reduces performance but also increases maintenance costs and causes operational delays. Furthermore, resonance, whereby the feeder's natural frequency coincides with its operating frequency, can result in damaging vibrations that reduce equipment lifespan [3].

This study focuses on linear vibrating feeders and is divided into four main sections. The first section outlines feeder models, optimization, and operation, and sets out the research objectives. It also discusses the influence of the Finite Element Method (FEM) on the study and the potential and limitations of using simulations to detect failures. The second section compares computer-aided engineering software and selects the most suitable option. The third section explains the results of the analyses and adjustments made and compares the findings of this study with those of others. The final section discusses the economic and manufacturing benefits, as well as the results of the study. This study emphasizes the importance of including vibro motor effects in the analysis, as these motors are a critical component of linear vibrating feeders that have been overlooked in other studies.

Existing research on linear vibrating feeders has largely focused on load conditions and static performance metrics, often overlooking the critical role of dynamic interactions caused by vibro motors. These motors generate centrifugal forces that not only produce vibratory motion and induce complex stresses and dynamic behaviors within the feeder structure. Understanding these interactions is vital for optimizing feeder designs and mitigating failure risks. This study addresses this gap by integrating static, modal, transient,

fatigue, and multi-body dynamics analyses to provide a comprehensive evaluation of the feeders. Each of these methods offers a distinct perspective on these complex systems.

1.1. Design and Optimization

The design process for vibrating feeders begins with simulating the feeder using FEM software [1-6]. Optimization is a mathematical strategy for determining the minimum or maximum values of a given function while taking a set of constraints into account. Optimizing machine components is essential for producing high-quality products at reduced cost. This method is commonly used to improve vibrating feeder designs, optimize frequency, and increase productivity [2, 7]. Several techniques aim to improve the vibrating feeder efficiency, including reducing energy consumption, increasing output, minimizing downtime, and simplifying maintenance. Yue-min et al. [3] found that adjusting the size of the stiffeners on the side plate while taking different frequency limits into account, improved the reliability of vibrating feeders.

1.2. Static Analysis of Vibrating Feeder

Finite Element Analysis (FEA) has become a powerful tool for simulating the structural and dynamic behavior of feeder components under various operating conditions [4]. In addition to FEA, Multibody Dynamics (MBD) simulation is becoming increasingly important in vibration analysis. It enables the modelling of complex interactions between moving parts, such as the feeder tray, springs, and exciters, and provides insight into system performance. The dynamic design of large vibrating feeders aims to improve reliability and longevity while maintaining economic and technical performance during normal operation [5].

Classical engineering principles, such as beam theory and finite element methods, derive analytical expressions for stress, deflection, and natural frequency [1]. FEA enables engineers to accurately model complex geometries, material properties, and loading conditions in order to predict stress, displacement, and deformation [6].

1.3. Modal Analysis of Vibrating Feeder

The boundary conditions in vibrating feeder systems include fixed supports, contact interfaces, and external loads on feeder trays and structural components. Ongoing research focuses on the integration of realistic material models, geometric nonlinearities, and dynamic loading on static behavior [8]. Modal analysis studies the dynamic effects of vibrating feeders under loading, focusing on resonant frequencies, mode shapes, and damping characteristics [9]. Experimental Modal Analysis (EMA) is widely used to characterize the dynamic behavior of vibrating feeders through physical testing [10]. FEA offers a powerful approach to modal analysis, enabling engineers to numerically simulate feeder dynamics [11].

Chandravanshi and Mukhopadhyay [12] used the FEM and EMA methods to investigate the effect of helical spring stiffness on feeder vibration, highlighting the influence of spring parameters on natural frequencies and mode shape. Zhu et al. [2] proposed a self-synchronous shaker with balanced elliptical motion and demonstrated improved performance through innovative design features. Oraon et al. [13] used FEA to perform diagnostic checks on vibrating feeder units, identifying potential structural weaknesses, and recommending design modifications to improve reliability and performance.

1.4. Transient Structural and Fatigue Life Analysis of Vibrating Feeder

Transient structural analysis focuses on the time-varying behavior of vibrating feeders under dynamic loading conditions, which is critical for assessing the structural integrity, dynamic response, and fatigue life during startup, shutdown, and transient operation [14]. Understanding transient behavior enables engineers to optimize feeder design and mitigate structural failures. FEA facilitates fatigue life analysis of vibrating feeders by allowing simulation of cyclic loading to evaluate structural response [15]. Guo et al. [6] conducted FEA of a dual-frequency vibrating screen, highlighting the importance of stress concentration analysis and fatigue life prediction in optimizing feeder design and improving reliability. Wang et al. [15] and Doğan et al. [16] analyzed the fatigue life of a large-scale linear vibrating feeder based on ANSYS. Their study emphasized the importance of accurate modeling of material properties, loading conditions, and boundary conditions for reliable fatigue life prediction.

A comprehensive investigation was conducted on a knockout machine in this study. The stress distribution and deformation of the vibrating feeder under static and dynamic loading were extensively evaluated. The vibrating feeder experiences severe vibration under high-intensity loads, increasing the risk of fatigue failure. The current design methods must be modified to accurately determine the resulting stress levels. This study is distinguished by the accurate simulation of the actual machine motion in ANSYS using real loading conditions. This one-to-one analysis allows for better evaluation of the results and clearer design changes, with the company confirming the modification's success.

2. Analysis of First Feeder

2.1. Preparations for Static Analysis

Two feeder designs were created using Computer Aided Design (CAD) software due to problems encountered during the manufacture and delivery of the first feeder. The second design incorporated customer feedback and resolved these issues. The study primarily aimed to perform extensive static and dynamic evaluations using ANSYS Workbench 2020 R2, taking into account as stp files opened in the ANSYS SpaceClaim service.

Several preparations were necessary to ensure accurate stress assessments in both feeder configurations. These preparations were identical for both feeders to facilitate a comparative analysis under the same boundary conditions. First, the geometry was cleaned to minimize elements that could negatively affect the meshing process. This involved removing all bolted connections from the geometry, replacing the CAD-specified springs with those added in ANSYS to enter their spring constants, and ignoring any damping effects. In addition, protective elements used only for transport were removed because the vibo motors complicated the design. Finally, all contact conditions were created and checked for correct meshing, resulting in 509 contacts for the first feeder. After assigning contact conditions, meshing operations were performed to create a mesh that accurately represented the system geometry and contact interfaces. Figure 1 shows the mesh geometry of the first feeder, which used various local meshing methods, including multizone, body sizing, and face sizing [17-19]. Based on the mesh independence results, an appropriate number of nodes (833,886) and number of elements (16,685) were selected.

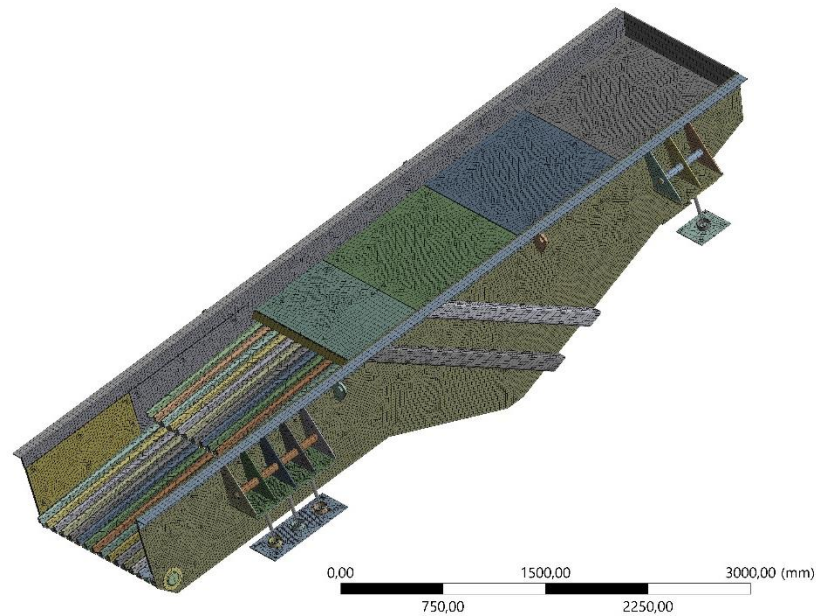


Figure 1. Meshed view of the first feeder

After meshing, the final preparations for the static analysis began. A force of 1,000 N each was applied to each plate to simulate the gravel load for processing. An additional 2,000 N was evenly distributed across the two grating layers at the front of the machine with 14 gratings in each layer, resulting in a force of 71.43 N per grating. Standard gravity was also applied in the -Z (vertical) direction. These setups correspond to practical field data from the equipment manufacturer, noting that there is no established protocol for testing or collecting data from machines with sensors.

2.2. Result of Static Analysis

Several key results, including total deformation, equivalent (von-Mises) stress, and spring probe data, were obtained from the ANSYS static analysis. The total deformation indicates the extent of the structural deformation under the applied loads, providing a comprehensive view of the displacement across the structure. This metric is critical for evaluating deflection and determining if the deformation remains within acceptable limits.

The equivalent stress (von-Mises) measures the stress state within the structure, considering all principal stresses (normal and shear stresses). This value helps engineers evaluate potential structural failure based on a single scalar value. By comparing the von-Mises stress to the yield strength of the material, engineers can assess whether the structure is operating within safe limits or at risk of failure. The equivalent stress (von-Mises) analysis results in Figure 2 show a maximum equivalent stress (von-Mises) of 595.11 MPa, observed at a small region, while the general stress distribution does not exceed 230 MPa, the yield strength of our material. The higher value of 595.11 MPa is probably due to spring modeling in the ANSYS Workbench.

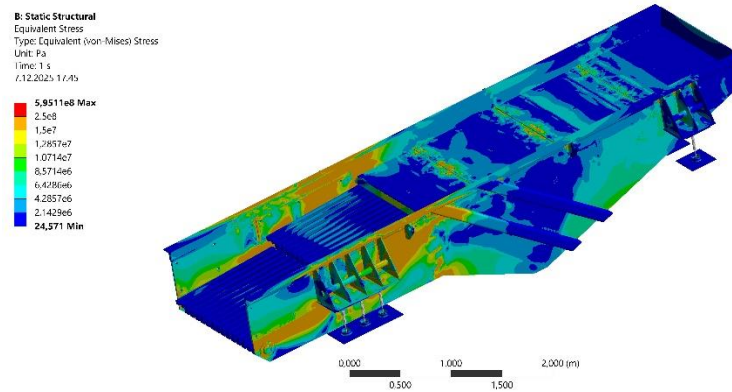


Figure 2. Static analysis - equivalent (von-Mises) stress

Figure 3 shows the spring probe data obtained from the analysis of the behavior of spring elements or connections within the structure. These data include spring forces, displacements, or stresses that are particularly relevant to assemblies or systems with components that exhibit spring-like behavior.

Details of "Spring Probe"	
Definition	
Type	Spring Probe
Boundary Condition	Longitudinal - BT-07-0202\Solid1 To BT-07-0202\...
Suppressed	No
Options	
Result Selection	All
<input type="checkbox"/> Display Time	End Time
Results	
<input type="checkbox"/> Elastic Force	-17652 N
<input type="checkbox"/> Damping Force	0, N
<input type="checkbox"/> Elongation	-46,01 mm
<input type="checkbox"/> Velocity	0, mm/s
Maximum Value Over Time	
<input type="checkbox"/> Elastic Force	-17652 N
<input type="checkbox"/> Damping Force	0, N
<input type="checkbox"/> Elongation	-46,01 mm
<input type="checkbox"/> Velocity	0, mm/s
Minimum Value Over Time	
<input type="checkbox"/> Elastic Force	-17652 N
<input type="checkbox"/> Damping Force	0, N
<input type="checkbox"/> Elongation	-46,01 mm
<input type="checkbox"/> Velocity	0, mm/s

Figure 3. Static analysis – spring probe

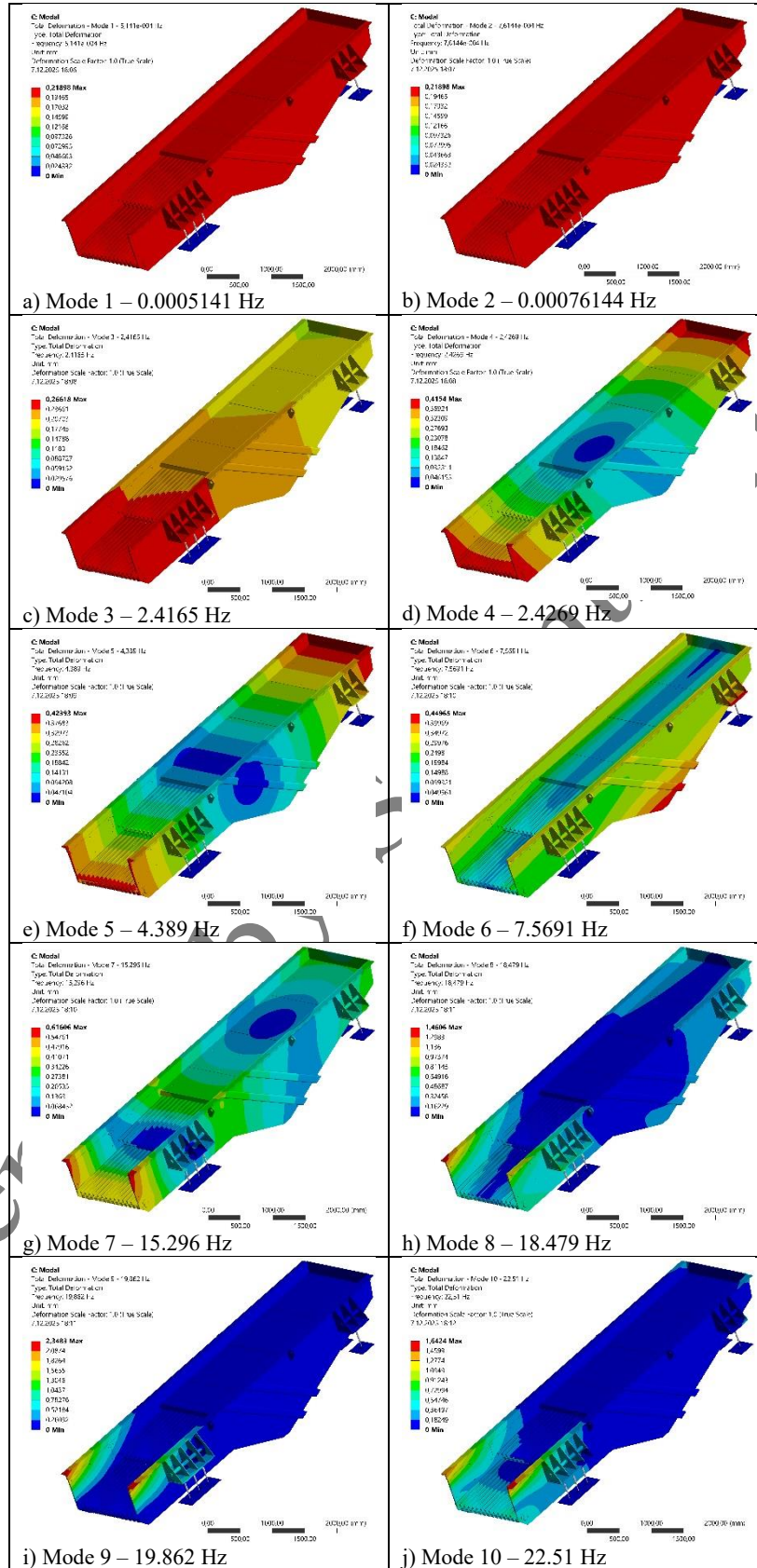
2.3. Modal Analysis

Modal analysis is a technique used to determine a structure or system's natural frequencies and mode shapes. Natural frequencies are the rates at which the structure tends to vibrate under dynamic loading, expressed in Hertz (Hz). Lower frequencies typically indicate larger, global deformations, whereas higher frequencies correspond to smaller, more localized vibrations.

Each frequency has a corresponding mode shape, which describes the pattern of deformation or vibration exhibited by the structure. Mode shapes provide insight into how different parts of a structure move relative to each other at a given frequency. Damping ratios quantify the amount of energy dissipated in each mode over time. Higher damping ratios indicate greater energy dissipation and faster vibration decay of vibrations, resulting in shorter transient responses. Identifying resonant frequencies is critical for avoiding potentially damaging vibrations and ensuring the structural integrity of the system.

Ten modes were identified in the modal analysis performed using ANSYS, and the results are shown in Table 1

Table 1. Modal analysis results of the first feeder



Modal analysis yields the effective mass to total mass data ratio for each system mode. This ratio determines how much each mode contributes to the system's dynamic behavior. This ratio shows how effective a mode is in a particular direction (usually in the X forward-backward, Y lateral, and Z vertical directions). The full value of the effective mass to total mass ratio is shown in Table 2.

Table 2. List of ratio of effective mass to total mass

Mode No.	X Direction	Y Direction	Z Direction
1	4.024E-03	0.98733	1.31E-14
2	0.98733	4.02E-03	6.00E-13
3	9.02E-13	3.20E-13	0.97058
4	2.46E-12	8.42E-11	5.74E+01
5	1.05E-13	6.72E-16	1.09E+02
6	2.68E-15	2.39E-13	1.56E-04
7	3.26E-15	1.99e-019	1.24E-04
8	2.05E-16	5.09E-15	8.16E-03
9	7.65E-17	1.06E-14	8.20E-01
10	1.65E-16	8.3731E-15	2.8604E-04
Sum	0.98734	0.98734	0.98732

The overall ratio value obtained as a result of the analysis is an indicator of how adequately all modes in the system are represented in terms of the dynamic response. This value shows the extent to which the modes considered in the modal analysis affect the system's total mass. In general, a total value close to 1 indicates that the modes considered in the modal analysis adequately cover the dynamic properties of the system and the results are reliable. In other words, the modes considered in the analysis effectively represent the system's vibration response. As shown in Table 2, most of the significant modes have been extracted in the modal analysis, as the sum of the total mass ratio in each direction exceeds 0.9873, thus bringing the total mass ratio close to 1. Therefore, to achieve the best possible balance between accuracy, processing time, and resources, the number of modes in this study was set at 10.

In the modal analysis performed in the ANSYS Workbench, the concept of mass participation in X, Y, and Z directions for natural frequencies calculated for each natural frequency expresses how much mass movement the system's vibration modes of the system generate in each direction. The results of the analysis are tabulated in Table 3 and can be used to understand which system modes dominate on which axis and are used to prevent or reduce unwanted vibrations in the design phase.

Table 3. Mass participation in X, Y and Z directions for natural frequencies

Mode No	Frequency (Hz)	Effective Mass (kg)		
		in X-Direction	in Y-Direction	in Z-Direction
1	0.0005	84.9	20,832.7	2.76E-10
2	0.0007	20,832.7	84.9	1.27E-08
3	2.4165	1.90E-08	6.74E-09	20,479.2
4	2.4269	5.19E-08	1.78E-06	121.2
5	4.3890	2.22E-09	1.42E-11	2.3
6	7.5691	5.65E-11	5.04E-09	3.3
7	15.2960	6.88E-11	4.20E-15	2.6
8	18.4790	4.33E-12	1.07E-10	172.3
9	19.8620	1.61E-12	2.24E-10	17,300.5
10	22.5100	3.48E-12	1.77E-10	6.0

The following conclusions can be drawn from Table 3:

- The total mass of the structure is 21,100 kg.
- A significant mass participation of 20,832.7 kg (98.7% of the total mass) is observed at a frequency of 0.0005387 Hz in the X forward-backward direction.
- A significant mass participation of 20,832.7 kg (98.7% of the total mass) is observed at a frequency of 0.0002753 Hz in the Y lateral direction.
- A significant mass participation of 20,479.2 kg (97.1% of the total mass) is observed at a frequency of 2.4165 Hz in the Z vertical direction [20-21].

Thus, Tables 2 and 3 show that modes 1, 2 and 3 are evidently the dominant modes in the lateral (Y), forward-backward (X) and vertical (Z) directions, respectively.

2.4. Transient Structural Analysis

Several key results were obtained from the transient structural study performed using ANSYS. This study also shows how the structure responds to dynamic loads over time. The study provides information on how the structure responds over time, including changes in displacement, velocity, acceleration, stress, and other response variables. Understanding the time-history response is essential for analyzing a structure's dynamic behavior and its ability to handle transient stresses. The stress distribution throughout the structure over time is presented, enabling stress levels to be compared with allowed limits and critical locations at risk of collapse to be identified. This information is vital for enhancing designs and ensuring structural integrity under transient stress conditions.

In this part, some dynamic forces are added to the boundary conditions alongside static forces. The vibro motor generates dynamic forces known as centrifugal forces. Figure 4 shows four moments representing the various orientations of the vibrating feeder's excitation force. The solid line arrows show the direction of the exciter force, and the dotted arrows show the direction of material movement. These four scenarios represent the maximum amplitude and speed of the vibrating feeder. The material force was close to its maximum when the exciter force was directed forwards and remained constant. The highest compression and tension forces occurred when the excitation force was oriented inwards and outwards. Therefore, these four moments may represent the vibrating feeder's limit conditions during the entire reciprocating vibration operation [14].

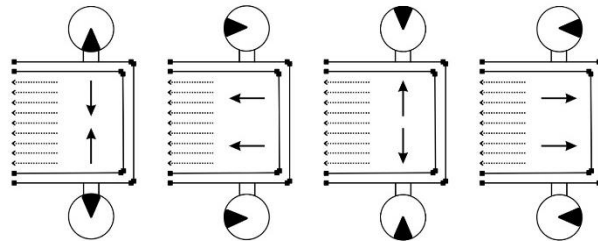


Figure 4. Directions of excitation force (centrifugal force) at four special moments. Respectively (left to right), backward and inward direction, same direction and forward, backward and outward, and same direction and backward

Since the vibro motor operates at 50 Hz, the dynamic force-time relationship was tabulated according to 50 Hz and transferred to ANSYS. Figures 5 and 6 show the boundary conditions and analysis settings for the transient structural analysis, respectively.

- E: Transient Structural**
 Transient
 Time: 5,e-003 s
 7.12.2025 17:48
- A** Force: 1000, N
 - B** Force 2: 1000, N
 - C** Force 3: 1000, N
 - D** Force 4: 1000, N
 - E** Force 5: 2000, N
 - F** Fixed Support
 - G** Force 6: 0, N
 - H** Force 7: 1,99e+005 N
 - I** Force 8: 1,99e+005 N
 - J** Standard Earth Gravity: 9,8066 m/s²

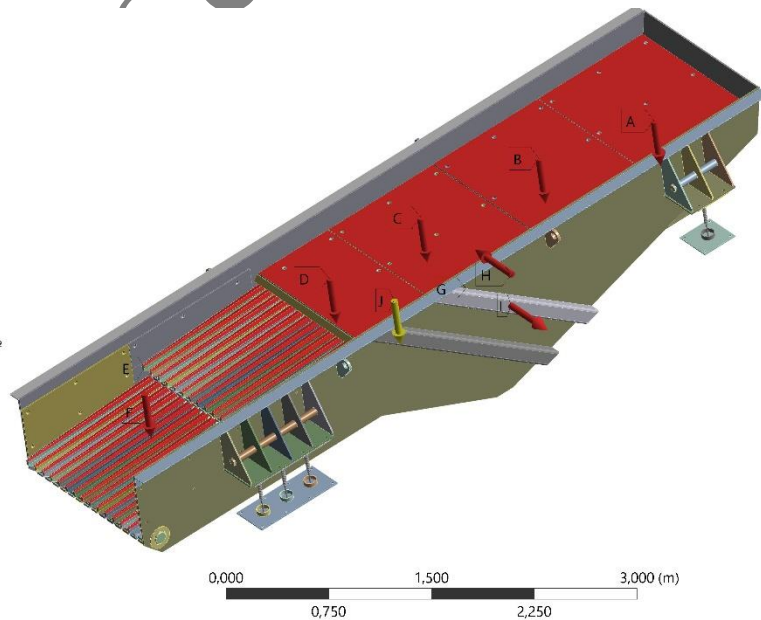


Figure 5. Boundary conditions of transient structural analysis

Details of "Analysis Settings"	
Step Controls	
Number Of Steps	1,
Current Step Number	1,
Step End Time	1, s
Auto Time Stepping	Off
Define By	Substeps
Number Of Substeps	200,
Time Integration	On
Solver Controls	
Solver Type	Direct
Weak Springs	Off
Large Deflection	Off
App. Based Settings	Moderate Speed Dynamics
Restart Controls	
Nonlinear Controls	
Advanced	
Output Controls	
Output Selection	None
Stress	Yes
Back Stress	No
Strain	Yes
Contact Data	Yes
Nonlinear Data	No
Nodal Forces	No
Volume and Energy	Yes
Euler Angles	Yes
General Miscellaneo...	No
Contact Miscellaneo...	No
Store Results At	All Time Points
Result File Compres...	Program Controlled
Damping Controls	
Stiffness Coefficient...	Direct Input
<input type="checkbox"/> Stiffness Coeffici...	0,
<input type="checkbox"/> Mass Coefficient	0,

ra Iranica

Figure 6. Transient structural analysis setting

The analysis generated a table showing equivalent stress results for 200-steps. The highest stress value for the maximum condition is 1541.4 MPa, and the lowest stress value is 80.306 MPa. For the minimum conditions, the highest stress value is 4.6156e-5 MPa, and the lowest stress value is 3.1879e-7 MPa. The maximum and minimum average stress values are 16.919 MPa, and 0.98827 MPa, respectively. The analysis also showed that the springs moved 40 mm forwards and backwards, and 90 mm upwards and downwards.

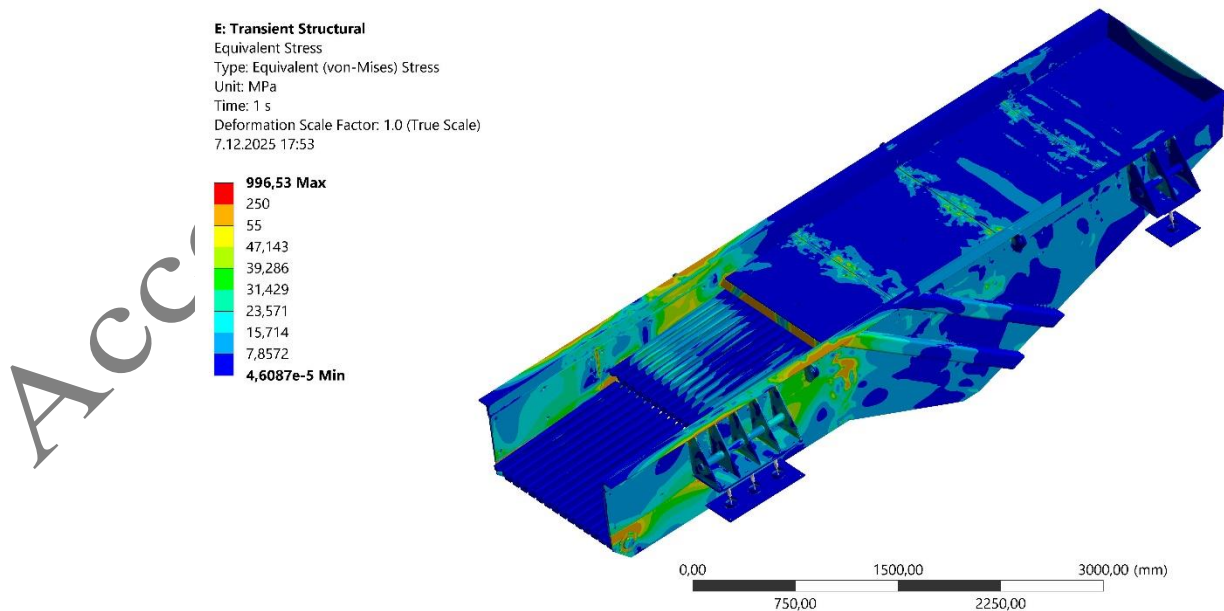


Figure 7. Result of transient structural analysis (equivalent stress)

As Figure 7 illustrates, the maximum stress value of 996.53 MPa was reached at 1 s for the second feeder.

2.5. Fatigue Life Analysis

The fatigue life analysis performed using ANSYS has provided several important results concerning the structural durability and service life of the structure under cyclic loading conditions. The most significant outcome is the prediction of the structure's life under cyclic loading. Engineers can use this information to calculate the number of cycles the structure can withstand before it fails due to fatigue, thereby helping them determine its durability and reliability. Fatigue life analysis also demonstrates that fatigue damage evolves by monitoring the fatigue crack initiation and propagation rates of fatigue cracks. This helps to identify potential failure mechanisms and optimize structural designs. It identifies critical areas of the structure where fatigue damage is most likely to occur, enabling engineers to implement mitigation techniques such as reworking components or optimizing material selection. The stress and strain distribution under cyclic loading conditions can be defined to help optimize designs and ensure structural integrity throughout the planned service life. Engineers then compare the predicted fatigue life with the required design life to determine the structure's safety factor against fatigue failure. This informs decisions regarding design specifications and fatigue mitigation strategies.

The "Mean Stress Curve" option in ANSYS's Mean Stress Theory has been used to evaluate the fatigue strength of the material under mean stress more accurately, as also recommended in ASTM E 1049-85 [23]. This curve shows how mean stress affects fatigue strength. It provides flexibility for different material types and loading conditions and is used to evaluate the effects of complex loading conditions and varying mean stress levels.

As shown in Figure 8, a fatigue analysis was performed to determine the service life, assuming a K_f value of 0.8. The K_f value, often referred to as "fatigue strength" or "fatigue strength reduction factor," is a coefficient that determines a material's resistance to a given stress level and how long it can withstand that stress. The K_f value for standard structural steels is found in the literature to be in the range of 0.8 - 0.6. Therefore, a K_f value of 0.8 was used in the analyses [22].

Using the mean stress curve in the analysis provides a more detailed and accurate understanding of how the mean stress affects the fatigue strength of the material, resulting in more reliable and accurate results.

Details of "Fatigue Tool"	
[-] Domain	
Domain Type	Time
[-] Materials	
Fatigue Strength Factor (Kf)	0,8
[-] Loading	
Type	Fully Reversed
<input type="checkbox"/> Scale Factor	1,
[-] Definition	
<input type="checkbox"/> Display Time	End Time
[-] Options	
Analysis Type	Stress Life
Mean Stress Theory	Mean Stress Curves
Stress Component	Equivalent (von-Mises)
[-] Life Units	
Units Name	cycles
1 cycle is equal to	1, cycles

Figure 8. Fatigue analysis settings

The feeder manufacturer reported that the first feeder failed after approximately one month. The fatigue life analysis determined that the break started after approximately 10^4 cycles. The lifespan is calculated based on the feeder operating for 12 hours per day using Equation 1 [10].

$$\frac{\text{Cycle}}{\text{Day}} = \frac{10^4 (\text{Cycle})}{12 \times 60 (\text{Hour/Day}) (\text{Minute})} = 13.9 \text{ Day} \quad (1)$$

The calculation showed that the feeder would fail due to vibration on the 13.9th day, and the life data is shown in Figure 9.

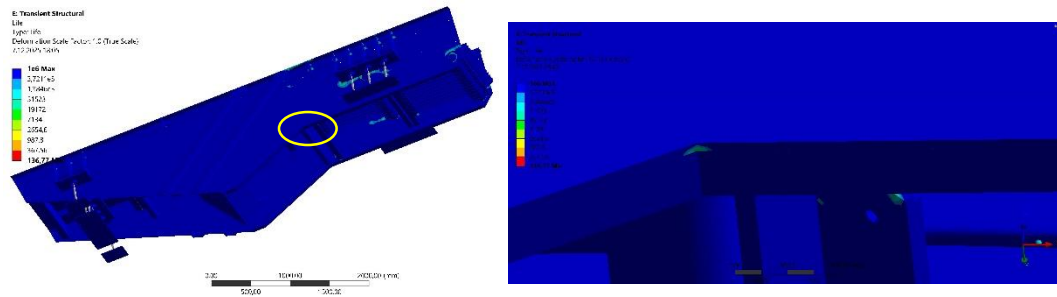


Figure 9. Result of transient structural – fatigue tool (life)

2.6. Effect of Meshing Process on Analysis

These analyses were conducted prior to completing the procedures in Sections 2.3, 2.4, and 2.5 using a mesh with fewer nodes and elements. As Chandravanshi and Mukhopadhyay [12] mentioned, 20 different meshes with varying numbers of elements were generated using the convergence principle to select the correct number of meshes, and the maximum stress values obtained from the static analysis were compared. These stress values were then combined with the number of nodes to produce convergence points, and the mesh structure with the minimum number of nodes was selected.

The aim of this study is to determine the correct number of meshes and avoid excessive CPU time, given that a geometry analysis involving a high mesh structure can take days or even weeks when our computers are running at maximum efficiency.

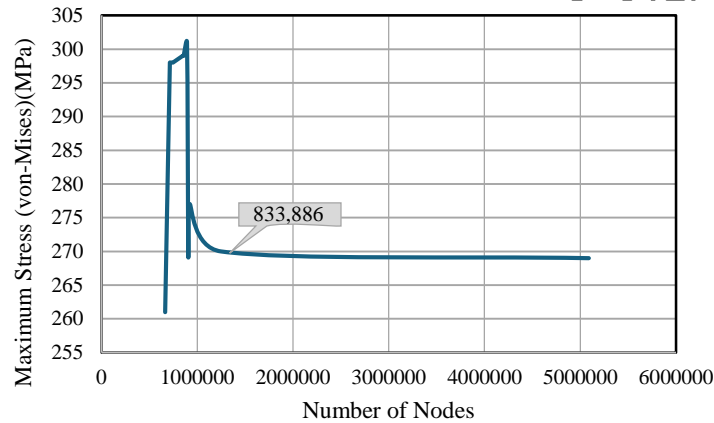


Figure 10. Maximum stress (von-Mises) vs number of nodes

Figure 10 shows that the minimum acceptable number of nodes is 833,886, with 166,857 elements.

3. Analysis of the Second Vibrating Feeder

3.1. Preparations for Static Analysis

This section presents the analysis of studies on the second on vibrating feeder. Design changes and additions were made to the second feeder to prevent stress accumulation and increase fatigue life by reducing the stress values at the breaking point. The second feeder was optimized and strengthened with additional side support profiles, as shown in Figure 11.

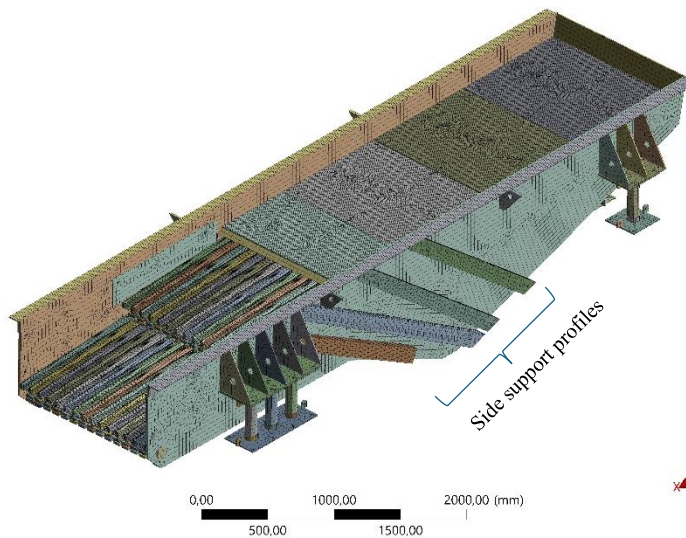


Figure 11. Meshed view of the second feeder with additional side support profiles

As shown in Figure 12, fillets were also added to the second vibrating feeder, indicated by the orange circle.

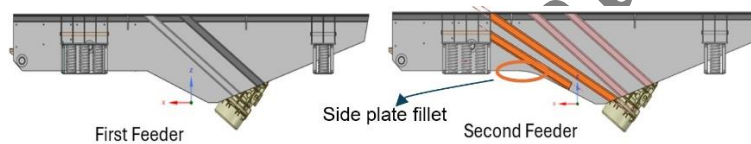


Figure 12. Illustration of the added supports

Based on the analysis results and the location of the fatigue failure, the thickness of the side plates and the diameter of the intermediate bars were increased, as shown in Figure 13 (orange circle).

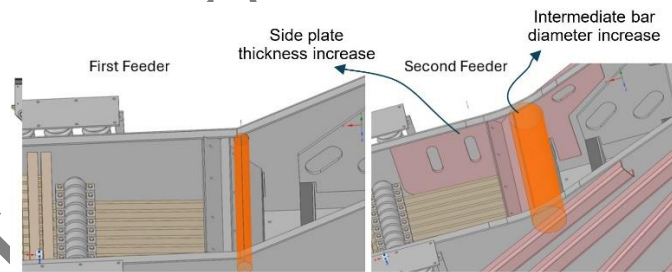


Figure 13. Reinforced version of the thicker side plate and increased intermediate circular part diameter in the second feeder

3.2. Static Analysis

In order to perform an accurate stress assessment, preparations were made for the second feeder configuration. These preparations were identical in order to enable proper comparison of the feeders. The boundary conditions were kept the same to enable proper comparison and evaluation of differences in the results.

To ensure that the mesh procedure was conducted correctly, the geometry cleaning technique was applied first, as before. This process minimizes the elements that could affect the mesh generation. As mentioned in Section 2.1, the entire preparation process was repeated for the second feeder. First, the bolts were removed, and then the springs were modelled in ANSYS. The elements protecting the springs were suppressed, and the density value of the material was finally adjusted.

Meshing operations were performed to generate an accurate geometric representation of the model. This meshing procedure ensures that the simulation accurately reflects the system's physical behavior. Figure 11 shows the mesh version of the feeder, consisting of 556,656 elements and 1,623,860 nodes.

As mentioned in Section 2.1, the final step of the static analysis was initiated once the meshing process had been completed. First, a force of 1,000 N was applied to each plate, in accordance with the company's specifications as described in Section 2.1. Next, a force of 71.43 N was applied to each plate, and the fixed supports were positioned. Standard gravity was also applied in the -Z (vertical) direction.

The ANSYS static analysis yielded several significant results, including total deformation, equivalent (von-Mises) stress, and spring probe data. Total deformation offers a comprehensive insight into displacement along the structure due to the applied forces, demonstrating the extent to which the structure deforms under load. This measurement is essential for evaluating the structure's movement or deflection and for determining whether the deformation is within acceptable limits.

Taking all primary stresses into account, including shear and normal stresses, the equivalent stress (von-Mises) quantifies the stress state within the structure. This scalar value helps engineers to evaluate the potential for structural failure. By comparing the von-Mises stress to the yield strength of the material, engineers can determine whether the feeder is operating within safe limits or is at risk of failure. As shown in Figure 14, the equivalent stress (von-Mises) analysis result found throughout the investigation was 557.74 MPa.

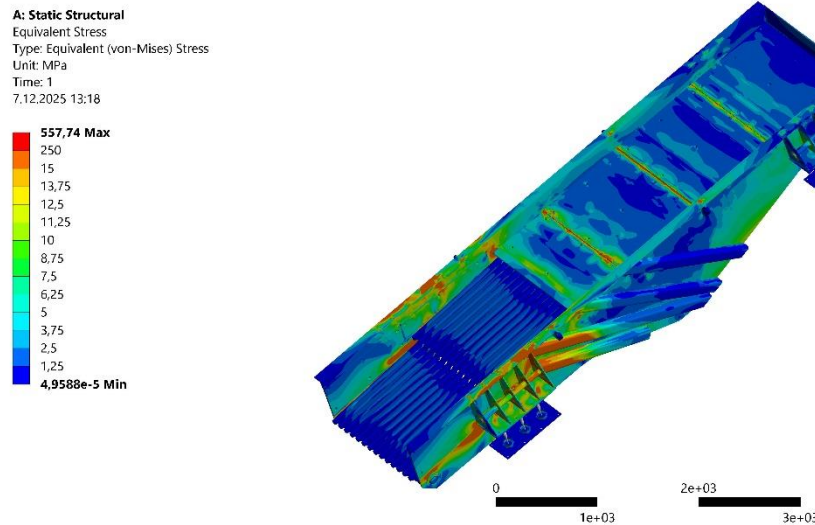


Figure 14. Static analysis of the second feeder equivalent stress (von-Mises)

The spring probe information shown in Figure 15 provides insight into the behavior of spring components or connections within the structure. This data includes information such as spring forces, displacements, and stresses, which help us to understand how components that behave like springs contribute to the structure's overall behavior, ensuring these components perform as intended. This is particularly important for assemblies or systems containing such components.

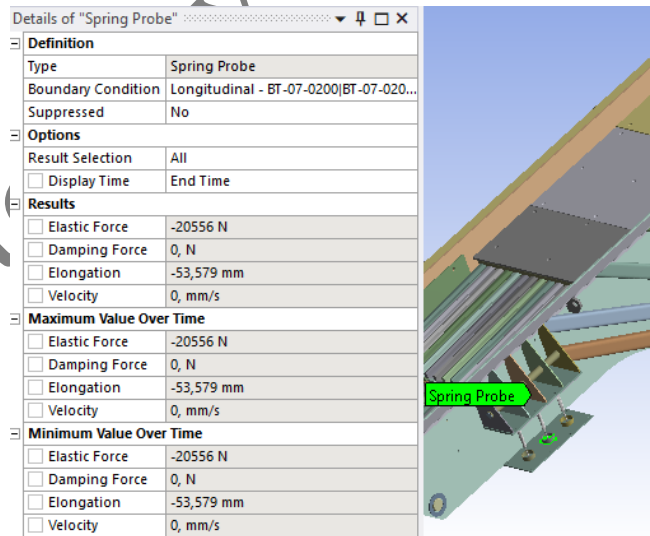


Figure 15. Static analysis of the second feeder - spring probe

3.3. Modal Analysis

As discussed in Section 2.3, modal analysis is a technique used to understand the dynamic response of a structure or system to nonlinear loads. The study involves identifying the eigenfrequencies, mode shapes, and damping ratios of the structure. A structure's eigenfrequencies represent its vibrational frequencies under dynamic loading. Finding resonant frequencies is essential to ensure the structural integrity of the system and avoid potentially damaging vibrations. The mode shapes represent the vibrations at each of the natural frequency.

To investigate these characteristics for the second feeder, a modal analysis study was performed using ANSYS software, focusing on the first ten mode shapes.

Table 4. Modal analysis of the second feeder

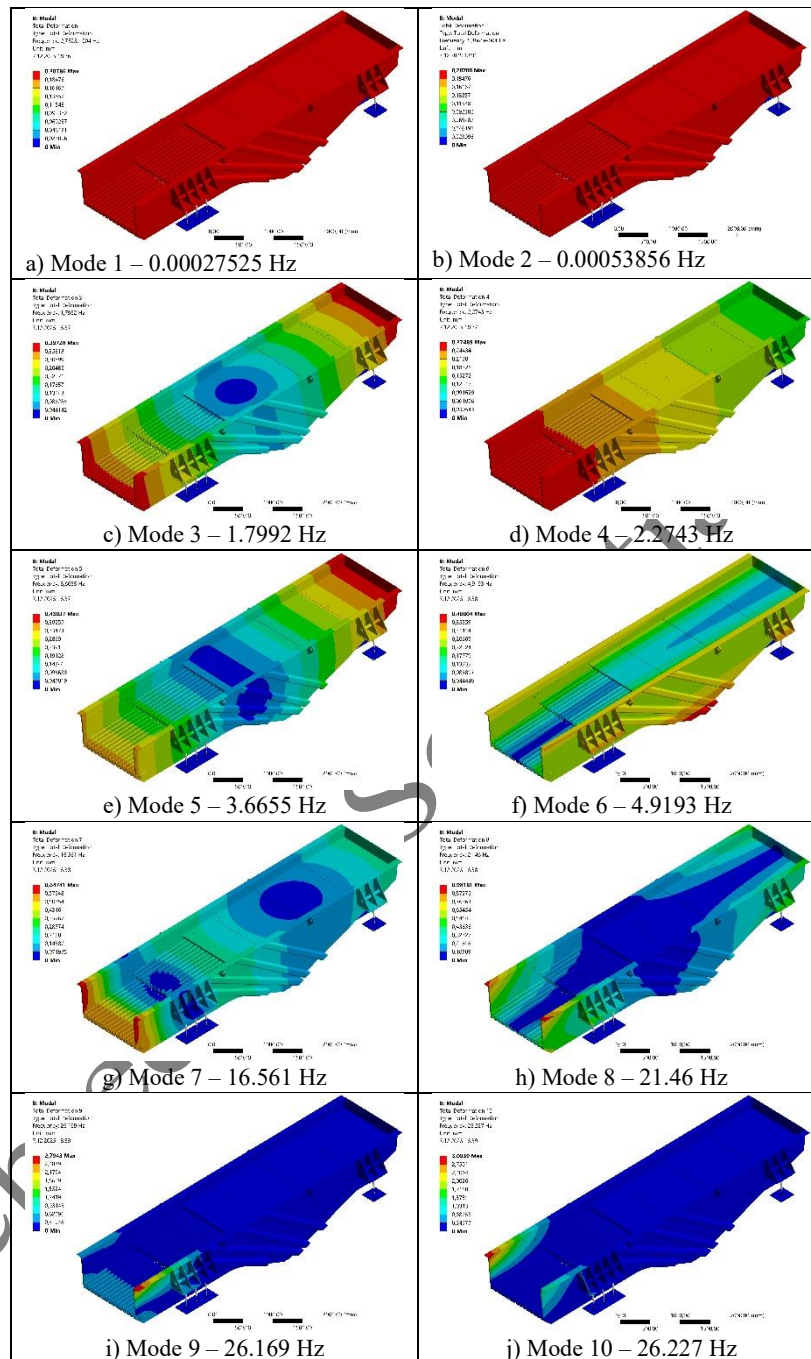


Table 4 shows the mode shapes generated for the second vibrating feeder at its natural frequencies. These mode shapes roughly represent the individual components of the vibrating feeder. According to the analysis results in

Table 5, the natural frequency values given by modes 4 and 5 are also close to the actual operating frequency of the feeder in the field. The value obtained for mode 5 can cause resonance.

One of the most important results of the modal analysis is the effective mass-to-total mass ratio data for each system mode. The complete set of ratios is shown in Table 5.

Table 5. List of ratio of effective mass to total mass

Mode No.	X Direction	Y Direction	Z Direction
1	3.87E-01	0.98856	6.13E-15
2	0.98856	3.87E-01	6.18E-14
3	2.09E-12	8.58E-12	1.98E-01
4	7.16E-14	3.88E-15	0.95785
5	2.20E-14	1.43E-15	3.07E+02
6	1.99E-16	4.13E-14	2.86E-03
7	1.22E-16	1.26E-15	5.90E-06
8	1.70E-19	6.79E-19	9.31E-05
9	4.46E-19	2.66E-16	2.26E-02
10	6.35E-18	2.02E-16	7.21E-02
Sum	0.9886	0.9886	0.9886

The modal analysis results examined in this study suggest that the total effective mass ratio is close to 1, indicating that the vibration characteristics of the system have been accurately captured and analyzed modes adequately represent the dynamic behavior. However, these results are subject to certain limitations and assumptions. Firstly, including insufficient modes in the modal analysis can affect the accuracy of the results. If an insufficient number of modes are included, some critical dynamic modes may be missed, reducing the reliability of the analysis. Therefore, a total effective mass ratio close to 1 does not necessarily guarantee that the modes fully reflect the system's dynamic characteristics. Increasing the number of modes can improve the accuracy of the analysis, particularly when low-frequency modes play a significant role in the system.

Since the total mass ratio in each direction adds up to 0.9886, or nearly 1, Table 5 shows that the modal analysis retrieved most of the relevant modes.

The effective mass ratios obtained in this study are generally consistent, particularly for low-frequency modes. However, additional analysis methods are recommended to verify the accuracy of the results for the high-frequency modes results in representing the system's actual dynamic behavior. Furthermore, modes with high total mass ratios may be the primary sources of vibration in the system, and controlling these modes could improve its dynamic performance [20-21].

Table 6. Mass participation in X-, Y- and Z- directions for natural frequencies

Mode No	Frequency (Hz)	Effective Mass (kg)		
		in X-Direction	in Y-Direction	in Z-Direction
1	0.0003	0.9	23,101.7	1.43E-10
2	0.0005	23,101.7	0.9	1.44E-09
3	1.7992	4.88E-08	2.00E-07	4,617.5
4	2.2743	1.67E-09	9.06E-11	22,384.0
5	3.6655	5.15E-10	3.33E-11	7.2
6	4.9193	4.64E-12	9.64E-10	66.8
7	16.5610	2.84E-12	2.95E-11	0.1
8	21.4600	3.98E-15	1.59E-14	2.2
9	26.1690	1.04E-14	6.21E-12	527.8
10	26.2270	1.48E-13	4.72E-12	1,685.9

The following conclusions can be drawn from Table 6:

- The total mass of the structure is 23,369 kg.
- A significant mass participation of 23,101.7 kg (98.8% of the total mass) is observed at a frequency of 0.00076144 Hz in the X forward-backward direction.
- A significant mass participation of 23,101.7 kg (98.8% of the total mass) is observed at a frequency of 0.0005141 Hz in the Y lateral direction.
- A significant mass participation of 22,385.4 kg (95.7% of the total mass) is observed at a frequency of 2.2743 Hz in the Z vertical direction [20-21].

Thus, Tables 5 and 6 show that modes 1, 2 and 4 in the lateral (Y), forward-backward (X) and vertical (Z) directions, respectively, are evidently dominant modes with considerable mass participation.

3.4. Transient Structural Analysis

A transient structural analysis was performed on the second feeder based on the objectives stated in Section 2.4. Conducted in ANSYS, this study examined the dynamic behavior of the mechanical system over time under different loading scenarios. The aim was to understand how the system responds to dynamic inputs.

The boundary conditions for the second feeder are shown in Figure 16. Force1 to Force5 represent static forces, while Force6 to Force8 represent dynamic forces. Force6 exerts both downward and upward forces, while Force7 and Force8 exert leftward and rightward forces, respectively.

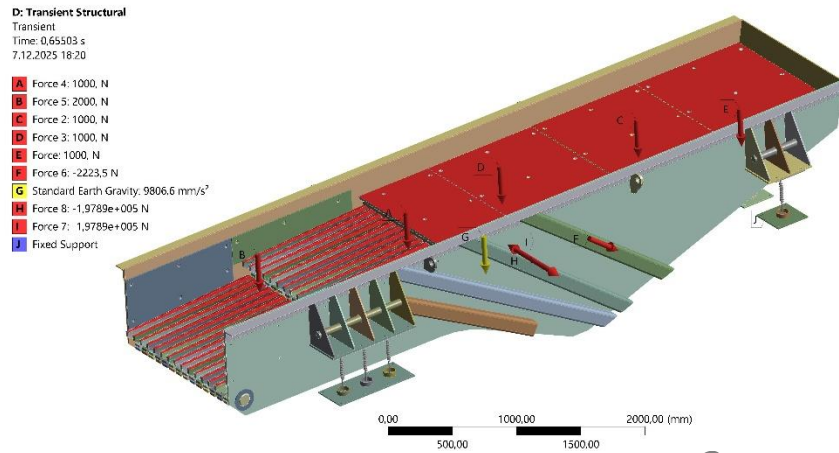


Figure 16. Boundary conditions of transient structural analysis for the second feeder

Analysis setting is shown in Figure 17.

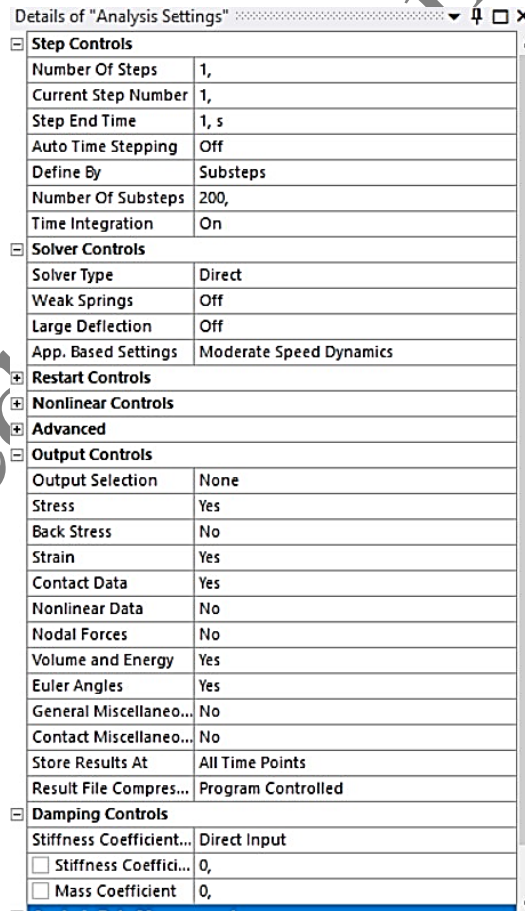


Figure 17. Analysis setting of transient structural analysis

The dynamic forces and time-force relationships were presented in tabular form at 50 Hz and transferred to ANSYS, as the vibro motor in the second feeder operated at this frequency. Based on the investigation, a table showing the equivalent stress results for the first feeder was generated in 200 steps. The maximum stress value was found to be 1,536.6 MPa, while the minimum stress value

was 107.04 MPa. For the minimum values, the lowest stress recorded was 1.5582×10^{-6} MPa, and the highest stress value was 6.1637×10^{-5} MPa. The highest and lowest average stress values were 14.095 MPa and 0.93728 MPa, respectively. The analysis showed that the movements caused the springs to displace 35 mm in both lateral directions and 120 mm vertically. Figure 18 shows the stress value for the second feeder at 0.165 seconds, which is 950.85 MPa.

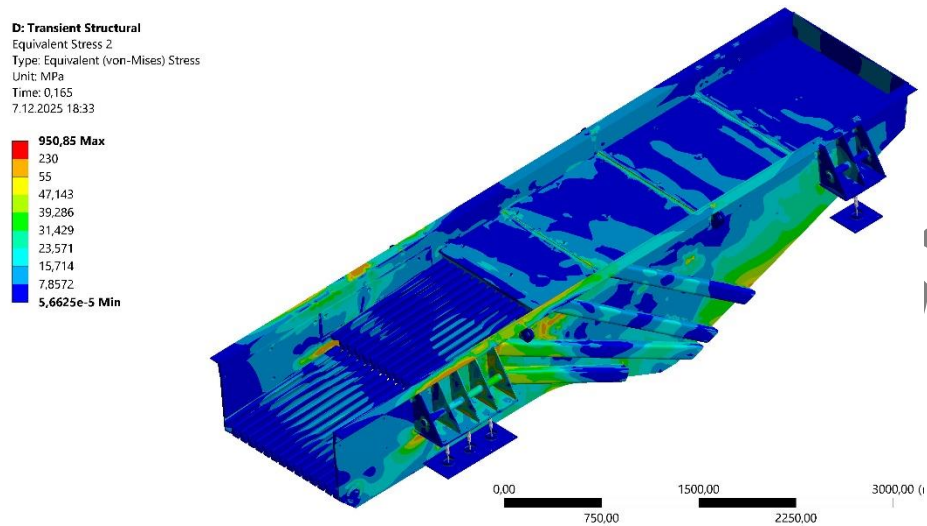


Figure 18. Result of transient structural analysis for the second feeder (equivalent stress-time: 0.165 seconds)

3.5. Fatigue Life Analysis

A fatigue analysis was performed on the second feeder using the methodology and techniques outlined in Section 2.5. The analysis revealed that the first feeder failed after 10^4 cycles during field use, whereas the second feeder reached 10^6 cycles at the same point. This suggests that, due to its improved design, the second feeder does not exhibit any signs of failure when the fatigue life curve is considered.

3.6. Effect of Feeder Meshing and Convergence Study on Analysis

A mesh independence study was performed similar to the one described in Section 2.6 was performed for the second feeder. As Chandravanshi and Mukhopadhyay [12] mentioned, different meshes with different element counts were generated using the convergence principle to select the appropriate mesh density. The maximum stress values obtained from the static analysis were then compared. As shown in Figure 19, node counts and stress values were combined to identify convergence points, and the mesh structure requiring the fewest nodes was selected. The purpose of this study, as stated in Section 2.6, is to minimize CPU time.

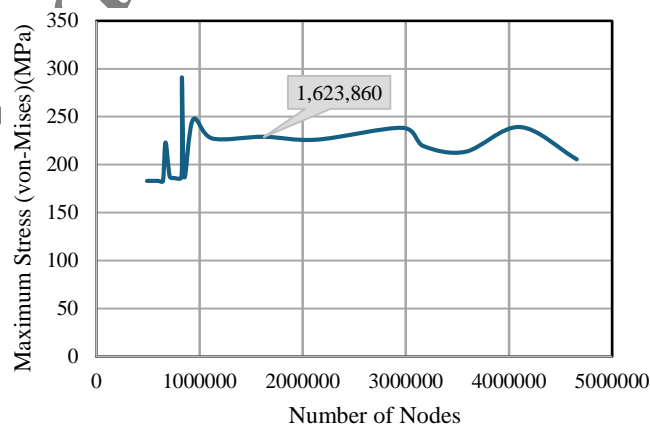


Figure 19. Maximum stress (von-Mises) vs number of nodes

As indicated by the grey label in Figure 19, the mesh structure with the fewest nodes where linearity occurs in the graph, was deemed sufficient for the mesh study. There are 1,623,860 nodes at this point.

4. Result and Discussion

The current study examined two different feeder designs. According to the feeder manufacturer, the first feeder became inoperable within a relatively short period of time due to fatigue failure of its side plates, as shown in Figure 20. Consequently, a revised second feeder was created that differed from the original. This included adding two additional side support profiles to each side plate, and replacing the sharp transition with a radius transition in the fractured area, and increasing the wall thickness and radius of the cylindrical portion under the gratings. It was later reported that the company's second feeder operated without failure at the sites to which it was sent.



Figure 20. Broken area of the first feeder

Thanks to its improved design, the second feeder functioned properly. Four critical evaluations were performed using static, modal, dynamic, and fatigue analyses. Error-free results were essential to ensure the applicability and real-world usability of these analyses. Many preparatory steps were meticulously carried out to ensure sensitive and accurate analyses, using the existing data, information, and documents provided by the equipment manufacturer.

Two different results were obtained from the static analysis: total deformation and equivalent stress (von-Mises). These results were then used to compare the two feeders. The high values recorded are largely due to the elongation of the springs. Figure 2 shows that the red and orange areas on the first feeder occupy more space than the corresponding areas on the second feeder in Figure 14. Additionally, it was observed that the second feeder exhibited less deformation at the back than the first feeder. Based on this analysis, it was concluded that, following the second feeder was more effective than the first. When the two feeders were compared, it was found that the stress distribution within the side walls of the first feeder was higher than that of the second. This difference is interpreted as being due to the additional side beams added in the second feeder, reducing the stress intensity on the walls. Furthermore, a decrease of approximately 58 MPa in the maximum stress values was observed in both feeders. The maximum stress in the fractured area of the first feeder was 142.38 MPa, whereas the maximum stress recorded in the second feeder was 84.495 MPa. This indicates that the design improvements made to the second feeder were effective.

Ten modal results were obtained from the modal analyses performed on both feeders. The natural frequency values of the first feeder ranged from 0.0003 Hz to 22.51 Hz, while those of the second feeder ranged from 0.0005 Hz to 26.227 Hz. Both feeders exhibited a critical natural frequency value in mode 7, which is significant given that their operating frequency is 15 Hz. One of the calculated natural frequency values is close to the operating frequency of the feeders, indicating potential resonance and failure if they continue to operate at this frequency. Notably, in mode 7, a high deformation value was observed at the very end of the grids, suggesting that the proximity of the general natural frequency values to the operating frequency could cause damage to the feeders, as shown in Figure 20.

The dynamic loads were categorized according to the centrifugal force of the vibro motor. The centrifugal force applied by each motor was then transferred to ANSYS. The feeder manufacturer verified the elliptical motion of the feeders, confirming that the elongation and shortening of the springs closely corresponded to the actual results. The maximum equivalent (von-Mises) stress obtained in the first feeder was 1,541.4 MPa, and the minimum value was 80.306 MPa. The highest and lowest average stresses were 16.919 MPa, and 0.98827 MPa, respectively. It was observed that the springs moved 40 mm laterally and 90 mm vertically due to the movements caused by the analysis. For the second feeder, the results were as follows: the maximum stress was 1,536.6 MPa, and the minimum was 107.04 MPa. The highest average stress was 14.095 MPa, and the lowest was 0.93728 MPa. The analysis showed that the movements caused the springs to displace by 35 mm laterally and 120 mm vertically. The higher results compared to the static analyses are believed to be due to the significant role of the centrifugal force from the vibro motors in the feeder's movement. Several factors contribute to the differences in results, including load application, time dependence, material behavior, inertial effects, and frequency effects [24-29].

A fatigue analysis was performed on the first and second feeders, producing different results. The first feeder experienced fatigue failure after 14 days of operation due to cyclic duplication exceeding the manufacturer's fatigue endurance limit, as calculated in Section 2.5. By contrast, the second feeder performed successfully up to 10^6 cycles and beyond. This difference highlights the

effectiveness of the design modifications made to the feeder. These revisions were intended to eliminate fatigue cracking, and the results of fatigue analysis suggest that these issues have been resolved.

Current studies have focused primarily on the load applied to the system, neglecting the most critical element: the vibro motor. The operational mechanisms of this motor and its effects are not well understood in the in current research literature. However, by focusing on this issue, it became clear that the vibro motor is a crucial component that had not been given sufficient consideration.

The analyses performed as part of this study, it was found that the total effective mass ratio for both feeders was close to 1, confirming that the analyzed modes adequately represented the overall vibration characteristics of the system [20].

The results of the study showed that the modes mostly had higher mass participation along the X and Y axes, indicating that the system is more dynamically active in these directions. This can be suppressed or controlled to improve the system's overall dynamic performance.

In general, vibro motors operate in a similar way to DC motors. The difference is in the hammers at both ends. The feeders lie in the hammers at both ends. These create through vibratory motion through the centrifugal force generated by the rotation of these parts. This motion then rolls and crushes the material placed on the linear vibrating feeder, transporting it to the next stage in the mobile jaw crusher. This study makes a substantial contribution to the analysis of linear vibrating feeders, an area that has received little attention in the literature up to this point, based on the findings of numerical and theoretical analysis [30].

5. Conclusions

This study involved a comparative analysis of two different feeder designs. The results showed that the second feeder's structural and operational performance was significantly better than that of the first feeder due to design modifications. A comparative analysis of the two industrial linear vibrating feeders revealed that static and dynamic performances of the second feeder were significantly enhanced.

Thanks to its enhanced design, which incorporates additional side support profiles, higher radius fillets at stress concentration points on the side plates, thickness increase at the side plates, and diameter increase at the intermediate bars, the second feeder's total deformation and equivalent stress (von-Mises) were revealed by static analysis to be reduced remarkably.

Modal analysis revealed that the natural frequencies of both feeders were close to the normal operating frequency of 15 Hz, posing a resonance risk. Consequently, the equipment manufacturer revised its recommended normal operating frequency from 15 Hz to 12 Hz.

Transient structural analysis revealed that the second feeder experienced lower maximum stress values and less spring movement due to the centrifugal force of the vibro motors, reflecting its superior design.

The fatigue analysis revealed a significant difference: the first feeder failed after 14 days, whereas the second feeder exhibited over 10^6 cycles, indicating enhanced design and manufacturing quality.

This study uniquely integrates static, modal, transient, fatigue, and multi-body dynamics analyses to provide a comprehensive view of feeder performance, an area not extensively covered in the existing literature. Multi-body dynamics analysis provides insight into the dynamic interactions of feeder components, enabling more accurate operational predictions. It can also accurately predict the response of a multi-body complex system, such as a dynamically running linear vibrating feeder.

Future research could involve exploring different operating conditions and material flows, evaluating alternative materials, and optimizing vibro motor configurations, with the aim of improving durability. Furthermore, strategies involving resonance control, smart materials [21], and real-time monitoring could enhance long-term performance. Investigating automation, energy-efficient designs, and multiphysics analysis would further improve our understanding of feeder behavior in complex scenarios.

In summary, the analysis of the failed first feeder revealed that the revised second feeder outperformed the first in all parameters. This demonstrates the effectiveness of the design improvements and highlights the importance of thorough analysis and an iterative design process for improving the performance and durability of mechanical components.

Acknowledgment

This study was partially supported by The Scientific and Technological Research Council of Turkey (TUBITAK) with the project under 2209-B University Students' Industry-Oriented Research Projects Support Program.

Authors' Credit

Efkan ŞENCAN: Data curation, Investigation, Methodology, Software, Writing – original draft

Yakup Taner TAŞDELEN: Data curation, Formal analysis, Investigation, Software, Validation, Writing – original draft, Writing – review & editing

Özge GÜLER: Conceptualization, Data curation, Investigation, Project administration, Writing – original draft, Writing – review & editing, Formal analysis, Validation

Paşa YAYLA: Conceptualization, Formal analysis, Investigation, Methodology, Project administration, Supervision, Writing – original draft, Writing – review & editing

Conflicts of interest

The authors declare that they have no known competing financial interests or personal relationships that could have appeared to influence the work reported in this paper.

References

- Ramatsetse, B. Mporfu, K., and Makinde, O. "Failure and sensitivity analysis of a reconfigurable vibrating screen using finite element analysis. Case Studies in Engineering" *Failure Analysis*, 9, 40-51, 2017. <https://doi.org/10.1016/j.csefa.2017.04.001>
- Zhu, W., Wang, H., and Dong, L. "Design and performance analysis of dual vibrating motors self synchronous shaker with balanced elliptical motion", *Applied Mechanics and Materials*, 284, 677-680, 2013. <https://doi.org/10.4028/www.scientific.net/AMM.284-287.677>
- Yue-min, Z., Chu-sheng, L., Xiao-mei, H., et al. "Dynamic design theory and application of large vibrating screen", *Procedia Earth and Planetary Science*, 1(1), 776-784, 2009. <https://doi.org/10.1016/j.proeps.2009.09.123>
- Li, L., Li, Y., Wang, J., et al. "Simulation study on the influence of variable frequency and input quantity on feeding ability of vibratory feeder", *Academic Journal of Manufacturing Engineering*, 17(3), 183-190, 2019.
- Zhang, Y. L., Liu, X. P., and Hou, C. L. "Key technology research on dynamic design of a large vibrating screen", *Applied Mechanics and Materials*, 709, 9-14, 2015. <https://doi.org/10.4028/wzhangww.scientific.net/AMM.709.9>
- Guo, N. Q., Liu, W., and Huang, W. P. "Finite element analysis of the screen box of the combined vibrating screen based on ANSYS", *Applied Mechanics and Materials*, 128, 1316-1320, 2012. <https://doi.org/10.4028/www.scientific.net/AMM.128-129.1316>
- Esmaceli Nezhad, A., and Samimi, M.H. "Investigation of transformer vibration characteristics using the finite element method", *Scientia Iranica*, 31(5), 441-457, 2024. <https://doi.org/10.24200/sci.2022.59006.6012>
- He, W. F., and Xian, A. M. "Statics and modal analysis for large vibrating screen", *Applied Mechanics and Materials*, 380, 136-139, 2013. <https://doi.org/10.4028/www.scientific.net/AMM.380-384.136>
- Zhang, L. W., Yin, Z. J., Chen, B., et al. "Dynamic simulation and experimental modal analysis of large vibratory feeder", *Advanced Materials Research*, 139, 2423-2426, 2010. <https://doi.org/10.4028/www.scientific.net/AMR.139-141.2423>
- Chandravanshi, M. L., and Mukhopadhyay, A. K. "Experimental modal analysis of the vibratory feeder and its structural elements", *International Journal of Applied Engineering Research*, 10(13), 33303-33310, 2015.
- Peng, C. Y., and Su, R. H. "Simulation applied to working frequency selection in large-scale vibrating screen's design", *Journal of Coal Science and Engineering (China)*, 17, 439-442, 2011. <https://doi.org/10.1007/s12404-011-0416-6>
- Chandravanshi, M. L., and Mukhopadhyay, A. K. "Analysis of variations in vibration behavior of vibratory feeder due to change in stiffness of helical springs using FEM and EMA methods", *Journal of the Brazilian Society of Mechanical Sciences and Engineering*, 39, 3343-3362, 2017. <https://doi.org/10.1007/s40430-017-0767-z>
- Oraon, S., Chandravanshi, M. L., and Bajpai, V. "Diagnosis check in the vibratory feeder unit using FEA technique", *Materials Today: Proceedings*, 16, 329-335, 2019. <https://doi.org/10.1016/j.matpr.2019.05.098>
- Xu, N. Wang, X., Yu, C., et al., "Structure optimization of vibrating feeder based on inertia release", *Shock and Vibration*, 1-13, 2021. <https://doi.org/10.1155/2021/8830882>
- Wang, Y., Fu, X., Guo, T., et al. "Fatigue life analysis of large-scale liner vibration screener based on ANSYS", *Applied Mechanics and Materials*, 37, 466-470, 2010. <https://doi.org/10.4028/www.scientific.net/AMM.37-38.466>
- Doğan, V.N., Çapar, M., Güler, Ö., et al. "Failure analysis and prevention of a heavy-duty industrial vibrating feeder". *J Fail. Anal. and Preven*, 24(4), 1788-1798, 2024. <https://doi.org/10.1007/s11668-024-01958-y>
- Saravanan, A., Sudharsan, G., Suresh, P.A., et al. "Performance study on a high-strength extruded magnesium alloy van frame using FEA", *Strength of Materials*, 55(6), pp.1297-1309, 2023. <https://doi.org/10.1007/s11223-024-00619-7>
- Kumar, K.S., Babu, J.M., Prakash, P.J., et al. "Modal analysis of natural rubber enhanced suspension system for vibration reduction". In *AIP Conference Proceedings* (Vol. 2715, No. 1), 2023. AIP Publishing. <https://doi.org/10.1063/5.0134135>
- Kumar, K.S., Arun, S., Mohan, A., et al. "Experimental analysis of noise and vibration reduction in windmill gear box for 5MW wind turbine", *Int J Mech Eng Technol (IJMET)*, 7(6), pp.76-85, 2016.

20. Ivancu, B., Voicu, G., Paun, A., et al. "Harmonic analysis of an vibrating feeder using "linear dynamics" module", *Proceedings of 43rd International Symposium on Agricultural Engineering: Actual Tasks on Agricultural Engineering*, Opatija, Croatia, 505-511, 2015.
21. Xia, X., Jing, W., Zhang, Z., et al. "Collaborative optimization of screening efficiency and screen surface load—Part I: Modeling and evaluation", *Particuology*, 69, 77-87, 2022. <https://doi.org/10.1016/j.partic.2021.11.006>
22. Parareda, S., Frómeta, D., Casellas, D., et al. "Understanding the fatigue notch sensitivity of high-strength steels through fracture toughness", *Metals*, 13(6), 1117, 2023. <https://doi.org/10.3390/met13061117>
23. ASTM E 1049-85 Standard practices for cycle counting in fatigue analysis, in: (1997). Anonymous (ed.), *Annual Book of ASTM Standards*, American Society for Testing and materials, 03.01 Philadelphia, pp. 710–718, 1999.
24. Bathe, K.J. *Finite Element Procedures*, 2nd Edition, Massachusetts; USA: Prentice Hall, Pearson Education, 2014.
25. Zienkiewicz, O.C., Taylor, R.L., and Zhu, J.Z. *The Finite Element Method: Its Basis and Fundamentals*, Elsevier, 2005.
26. Kumar, A., and Harmain, G. "Revisiting the crack closure and its effect on fatigue life of components", *Sigma Journal of Engineering and Natural Sciences*, 42(2), 590-599, 2024. <https://doi.org/10.14744/sigma.2024.00046>
27. Atar, B., Üyüklü, E., and Yayla, P. "Microstructure and mechanical properties of an additively manufactured AlSi10Mg based alloy", *Materials Testing*, 65(6), 874-885, 2023. <https://doi.org/10.1515/mt-2022-0334>
28. Nikkhoo, A., Banihashemi, S., and Kiani, K. "Parametric investigations into dynamics of cracked thin rectangular plates excited by a moving mass", *Scientia Iranica*, 30(3), 860-876, 2023. <https://doi.org/10.24200/sci.2022.58345.5686>
29. Nikkhoo, A., Banihashemi, S., and Kiani, K. "On non-stationary response of cracked thin rectangular plates acted upon by a moving random force", *Scientia Iranica*, 2025. <https://doi.org/10.24200/sci.2023.61247.7220>
30. Linhares, T.B., da Silva Scari, A., and Vimieiro, C.B.S. "Causes of failures in vibrating screens: a literature review", *Minerals Engineering*, 218, 109027, 2024. <https://doi.org/10.1016/j.mineng.2024.109027>

Biographies

Efekan ŞENCAN graduated from the Marmara University Mechanical Engineering Department-Istanbul Türkiye. He has been working as a design and simulation engineer in a company in Türkiye.

Yakup Taner TAŞDELEN graduated from the Mechanical Engineering Department of Marmara University, Istanbul, Turkey. He has been working as a design engineer in a company in Türkiye.

Ozge GULER graduated from the Yeditepe University Mechanical Engineering Department-Istanbul Türkiye. She has been working in R&D project management, finite element analysis, machine design and manufacturing, together with CNC cutting processes, CAD&CAM programming, automation, manufacturing, and startup of agrega crushing, screening, and washing equipment, welding, and special manufacturing for over 10 years.

Pasa YAYLA graduated from the Istanbul Technical University Mechanical Engineering Department, Istanbul Türkiye. After getting his MSc degree from the same department, he pursued his PhD study in the Mechanical Engineering Department of Imperial College of Science, Technology and Medicine-University of London. Currently, he has been working as a professor at Marmara University, Engineering Faculty, Mechanical Engineering Department. His main research interests are fracture mechanics, structural integrity, and mechanics of materials.

Figure Captions

Figure 1. Meshed view of the first feeder

Figure 2. Static analysis - equivalent (von-Mises) stress

Figure 3. Static analysis – spring probe

Figure 4. Directions of excitation force (centrifugal force) at four special moments. Respectively (left to right), backward and inward direction, same direction and forward, backward and outward, and same direction and backward

Figure 5. Boundary conditions of transient structural analysis

Figure 6. Transient structural analysis setting

Figure 7. Result of transient structural analysis (equivalent stress)

Figure 8. Fatigue analysis settings

Figure 9. Result of transient structural – fatigue tool (life)

Figure 10. Maximum stress (von-Mises) vs number of nodes

Figure 11. Meshed view of the second feeder with additional side support profiles

Figure 12. Illustration of the added supports

Figure 13. Reinforced version of the thicker side plate and increased intermediate circular part diameter in the second feeder

Figure 14. Static analysis of the second feeder equivalent stress (von-Mises)

Figure 15. Static analysis of the second feeder - spring probe

Figure 16. Boundary conditions of transient structural analysis for the second feeder

Figure 17. Analysis setting of transient structural analysis

Figure 18. Result of transient structural analysis for the second feeder (equivalent stress-time: 0.165 seconds)

Figure 19. Maximum stress (von-Mises) vs number of nodes

Figure 20. Broken area of the first feeder

Table Captions

Table 1. Modal analysis results of the first feeder

Table 2. List of ratio of effective mass to total mass

Table 2. Mass participation in X, Y and Z directions for natural frequencies

Table 4. Modal analysis of the second feeder

Table 5. List of ratio of effective mass to total mass

Table 6. Mass participation in X-, Y- and Z- directions for natural frequencies

Accepted by Scientia Iranica

Figures

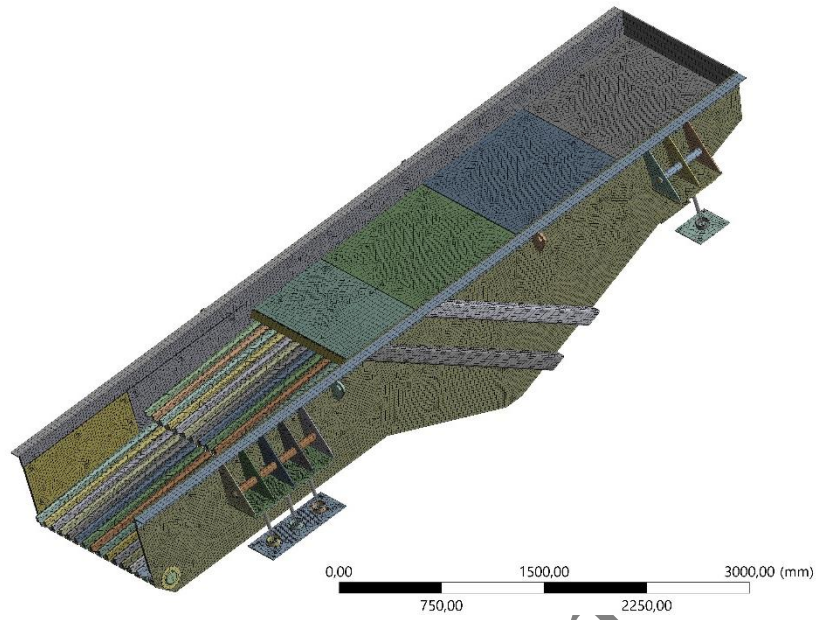


Figure 1. Meshed view of the first feeder

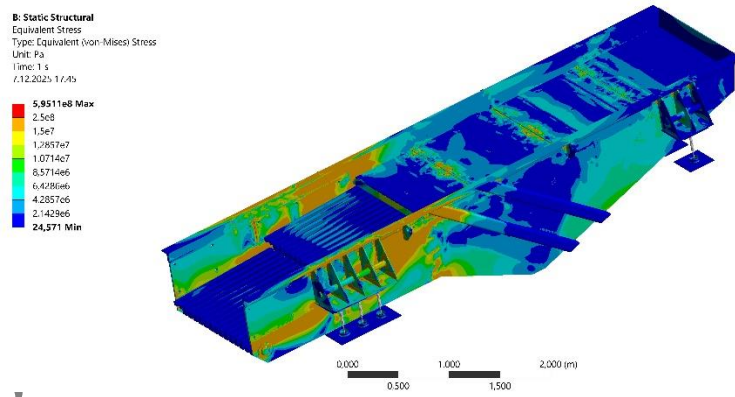


Figure 2. Static analysis - equivalent (von-Mises) stress

Details of "Spring Probe"	
Definition	
Type	Spring Probe
Boundary Condition	Longitudinal - BT-07-0202\Solid1 To BT-07-0202\...
Suppressed	No
Options	
Result Selection	All
<input type="checkbox"/> Display Time	End Time
Results	
<input type="checkbox"/> Elastic Force	-17652 N
<input type="checkbox"/> Damping Force	0, N
<input type="checkbox"/> Elongation	-46,01 mm
<input type="checkbox"/> Velocity	0, mm/s
Maximum Value Over Time	
<input type="checkbox"/> Elastic Force	-17652 N
<input type="checkbox"/> Damping Force	0, N
<input type="checkbox"/> Elongation	-46,01 mm
<input type="checkbox"/> Velocity	0, mm/s
Minimum Value Over Time	
<input type="checkbox"/> Elastic Force	-17652 N
<input type="checkbox"/> Damping Force	0, N
<input type="checkbox"/> Elongation	-46,01 mm
<input type="checkbox"/> Velocity	0, mm/s

Figure 3. Static analysis – spring probe

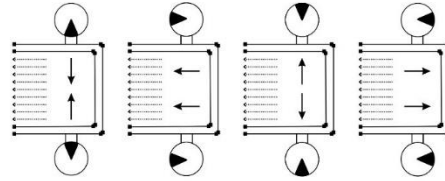


Figure 4. Directions of excitation force (centrifugal force) at four special moments. Respectively (left to right), backward and inward direction, same direction and forward, backward and outward, and same direction and backward

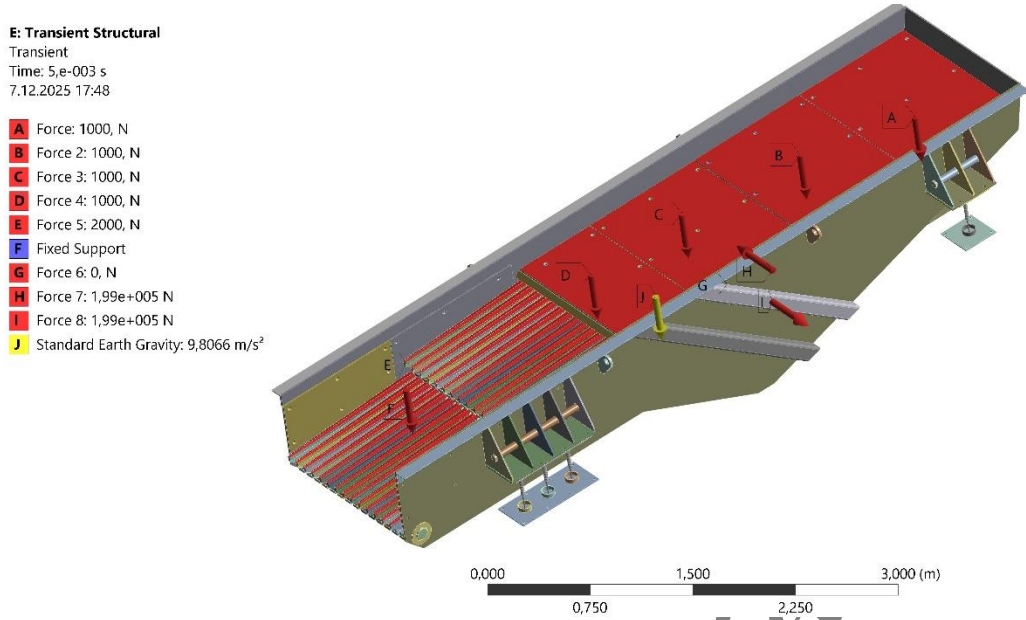


Figure 5. Boundary conditions of transient structural analysis

Details of "Analysis Settings"

Step Controls	
Number Of Steps	1,
Current Step Number	1,
Step End Time	1, s
Auto Time Stepping	Off
Define By	Substeps
Number Of Substeps	200,
Time Integration	On
Solver Controls	
Solver Type	Direct
Weak Springs	Off
Large Deflection	Off
App. Based Settings	Moderate Speed Dynamics
Restart Controls	
Nonlinear Controls	
Advanced	
Output Controls	
Output Selection	None
Stress	Yes
Back Stress	No
Strain	Yes
Contact Data	Yes
Nonlinear Data	No
Nodal Forces	No
Volume and Energy	Yes
Euler Angles	Yes
General Miscellaneo...	No
Contact Miscellaneo...	No
Store Results At	All Time Points
Result File Compres...	Program Controlled
Damping Controls	
Stiffness Coefficient...	Direct Input
<input type="checkbox"/> Stiffness Coeffici...	0,
<input type="checkbox"/> Mass Coefficient	0,

Figure 6. Transient structural analysis setting

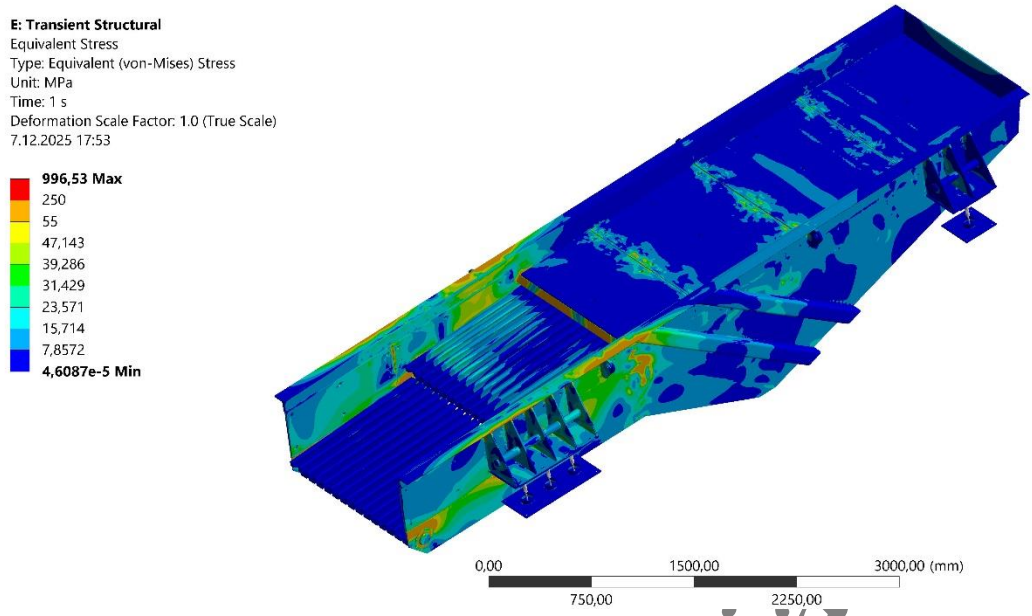


Figure 7. Result of transient structural analysis (equivalent stress)

Details of "Fatigue Tool" :

Domain	
Domain Type	Time
Materials	
Fatigue Strength Factor (Kf)	0,8
Loading	
Type	Fully Reversed
<input type="checkbox"/> Scale Factor	1,
Definition	
<input type="checkbox"/> Display Time	End Time
Options	
Analysis Type	Stress Life
Mean Stress Theory	Mean Stress Curves
Stress Component	Equivalent (von-Mises)
Life Units	
Units Name	cycles
1 cycle is equal to	1, cycles

Figure 8. Fatigue analysis settings

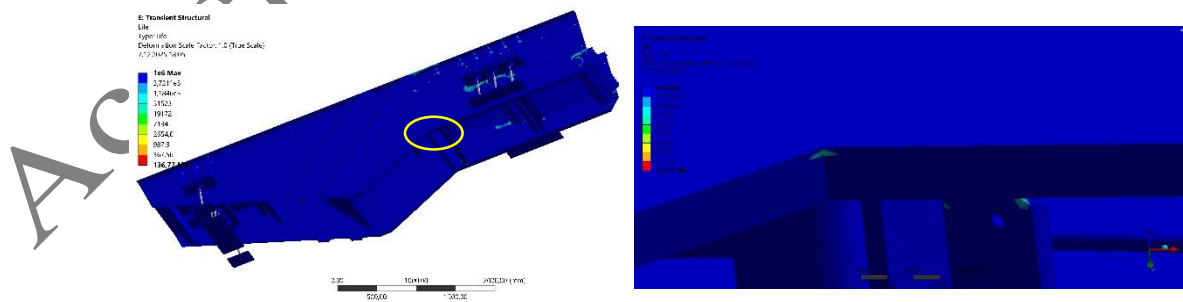


Figure 9. Result of transient structural – fatigue tool (life)

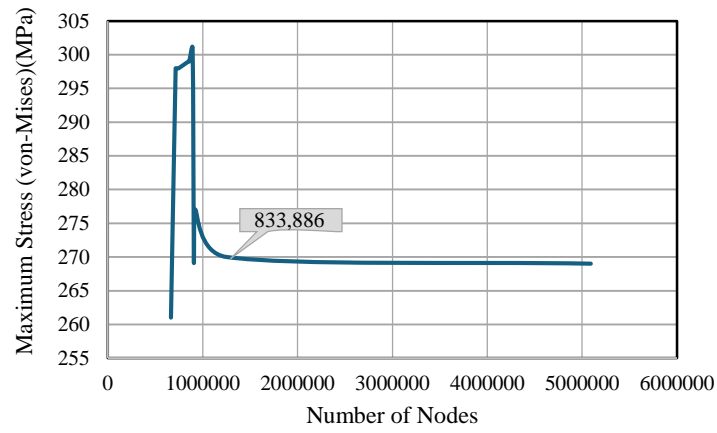


Figure 10. Maximum stress (von-Mises) vs number of nodes

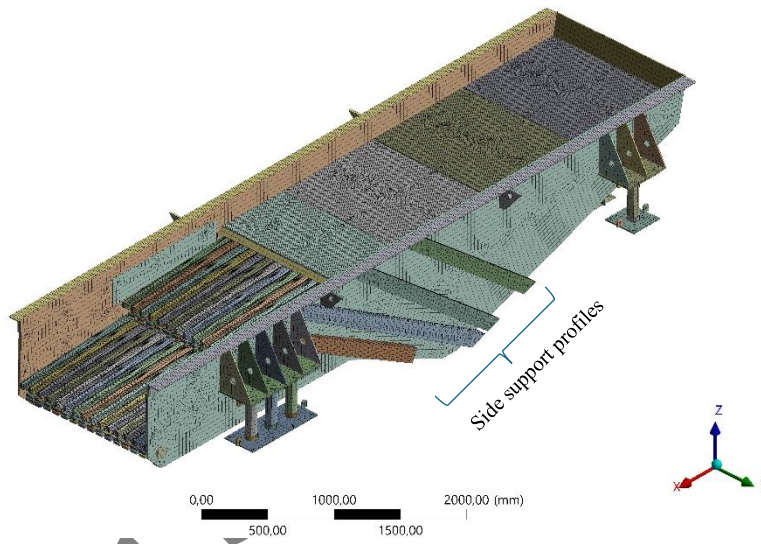


Figure 11. Meshed view of the second feeder

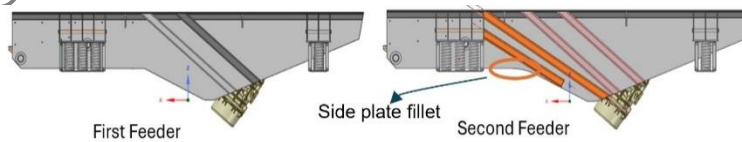


Figure 12. Illustration of the added supports

Iranica

Accepted

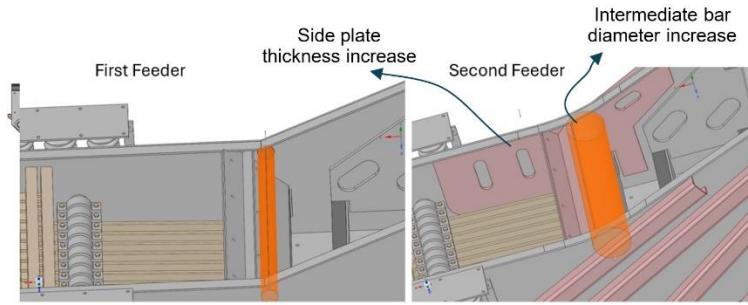


Figure 13. Reinforced version of the thicker side plate and increased intermediate circular part diameter in the second feeder

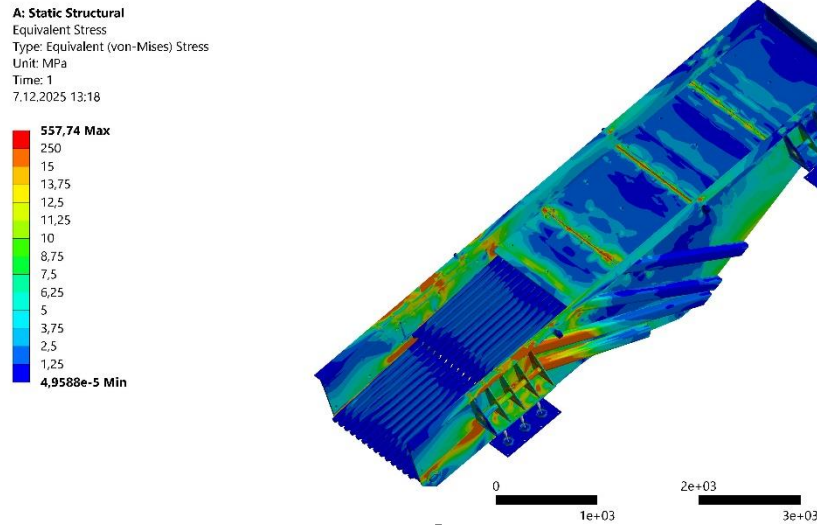


Figure 14. Static analysis of the second feeder equivalent stress (von-Mises)

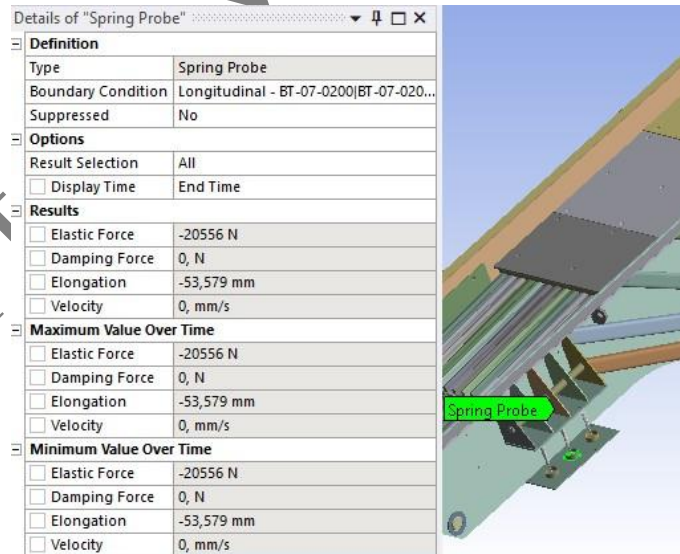


Figure 15. Static analysis of the second feeder - spring probe

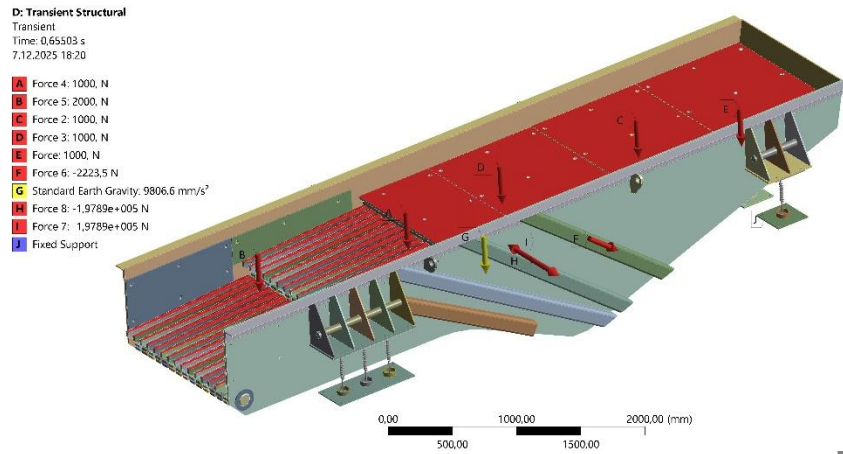


Figure 16. Boundary conditions of transient structural analysis for the second feeder

Details of "Analysis Settings"

Step Controls	
Number Of Steps	1,
Current Step Number	1,
Step End Time	1, s
Auto Time Stepping	Off
Define By	Substeps
Number Of Substeps	200,
Time Integration	On
Solver Controls	
Solver Type	Direct
Weak Springs	Off
Large Deflection	Off
App. Based Settings	Moderate Speed Dynamics
Restart Controls	
Nonlinear Controls	
Advanced	
Output Controls	
Output Selection	None
Stress	Yes
Back Stress	No
Strain	Yes
Contact Data	Yes
Nonlinear Data	No
Nodal Forces	No
Volume and Energy	Yes
Euler Angles	Yes
General Miscellaneo...	No
Contact Miscellaneo...	No
Store Results At	All Time Points
Result File Compres...	Program Controlled
Damping Controls	
Stiffness Coefficient...	Direct Input
<input type="checkbox"/> Stiffness Coeffici...	0,
<input type="checkbox"/> Mass Coefficient	0,

Figure 17. Analysis setting of transient structural analysis

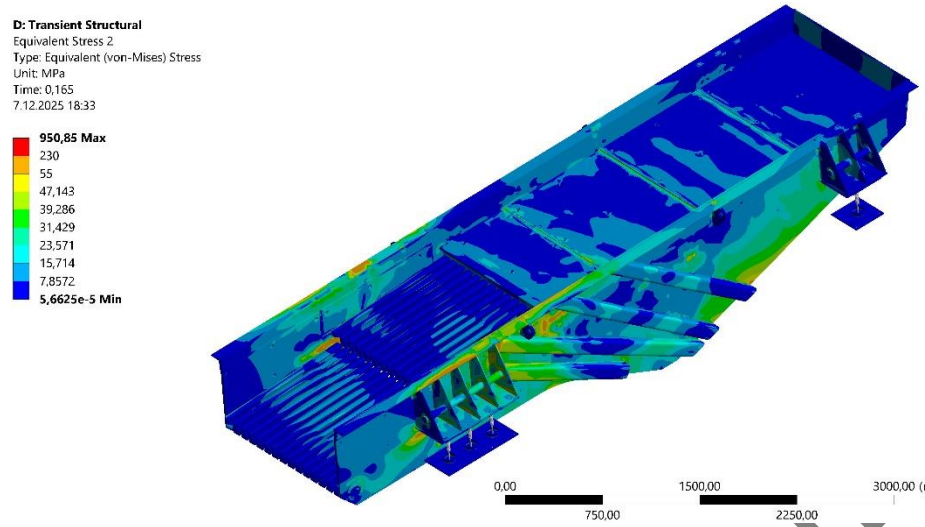


Figure 18. Result of transient structural analysis for the second feeder (equivalent stress-time: 0.165 seconds)

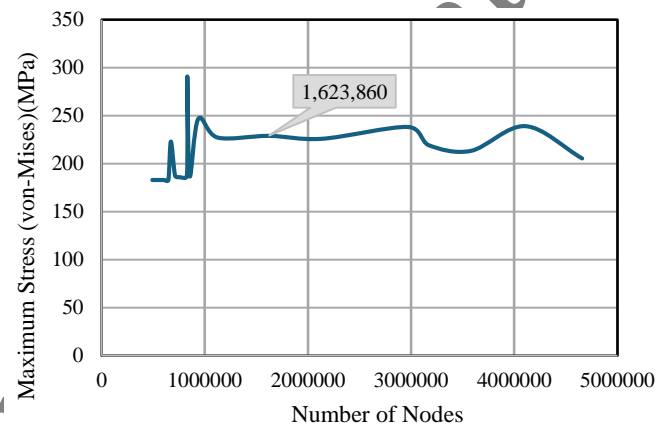


Figure 19. Maximum stress (von-Mises) vs number of nodes



Figure 20. Broken area of the first feeder

Tables

Table 3. Modal analysis results of the first feeder

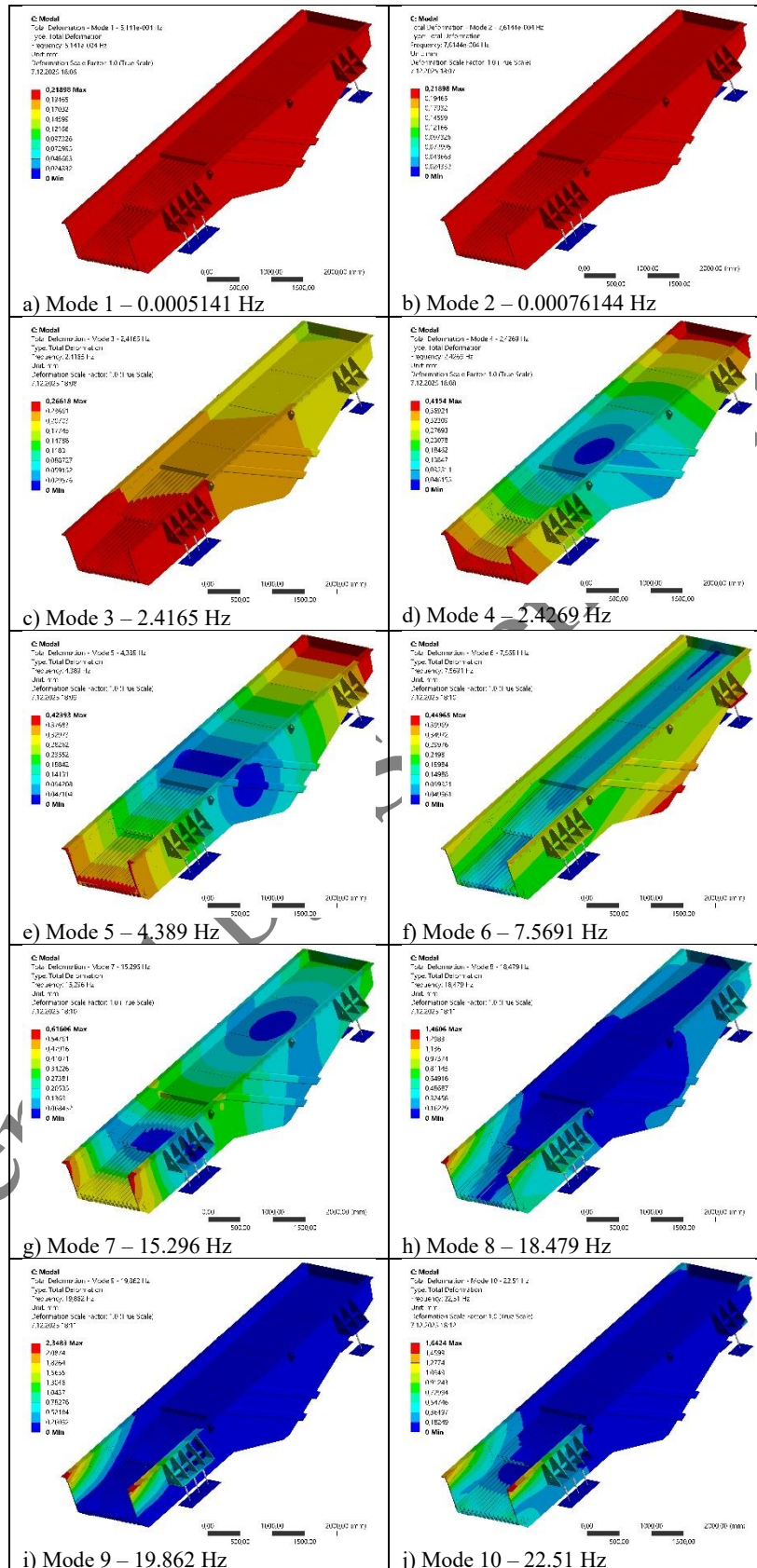


Table 4. List of ratio of effective mass to total mass

Mode No.	X Direction	Y Direction	Z Direction
1	4.024E-03	0.98733	1.31E-14
2	0.98733	4.02E-03	6.00E-13
3	9.02E-13	3.20E-13	0.97058
4	2.46E-12	8.42E-11	5.74E+01
5	1.05E-13	6.72E-16	1.09E+02
6	2.68E-15	2.39E-13	1.56E-04
7	3.26E-15	1.99e-019	1.24E-04
8	2.05E-16	5.09E-15	8.16E-03
9	7.65E-17	1.06E-14	8.20E-01
10	1.65E-16	8.3731E-15	2.8604E-04
Sum	0.98734	0.98734	0.98732

Table 5. Mass participation in X, Y and Z directions for natural frequencies

Mode No	Frequency (Hz)	Effective Mass (kg)		
		in X-Direction	in Y-Direction	in Z-Direction
1	0.0005	84.9	20,832.7	2.76E-10
2	0.0007	20,832.7	84.9	1.27E-08
3	2.4165	1.90E-08	6.74E-09	20,479.2
4	2.4269	5.19E-08	1.78E-06	121.2
5	4.3890	2.22E-09	1.42E-11	2.3
6	7.5691	5.65E-11	5.04E-09	3.3
7	15.2960	6.88E-11	4.20E-15	2.6
8	18.4790	4.33E-12	1.07E-10	172.3
9	19.8620	1.61E-12	2.24E-10	17,300.5
10	22.5100	3.48E-12	1.77E-10	6.0

Table 4. Modal analysis of the second feeder

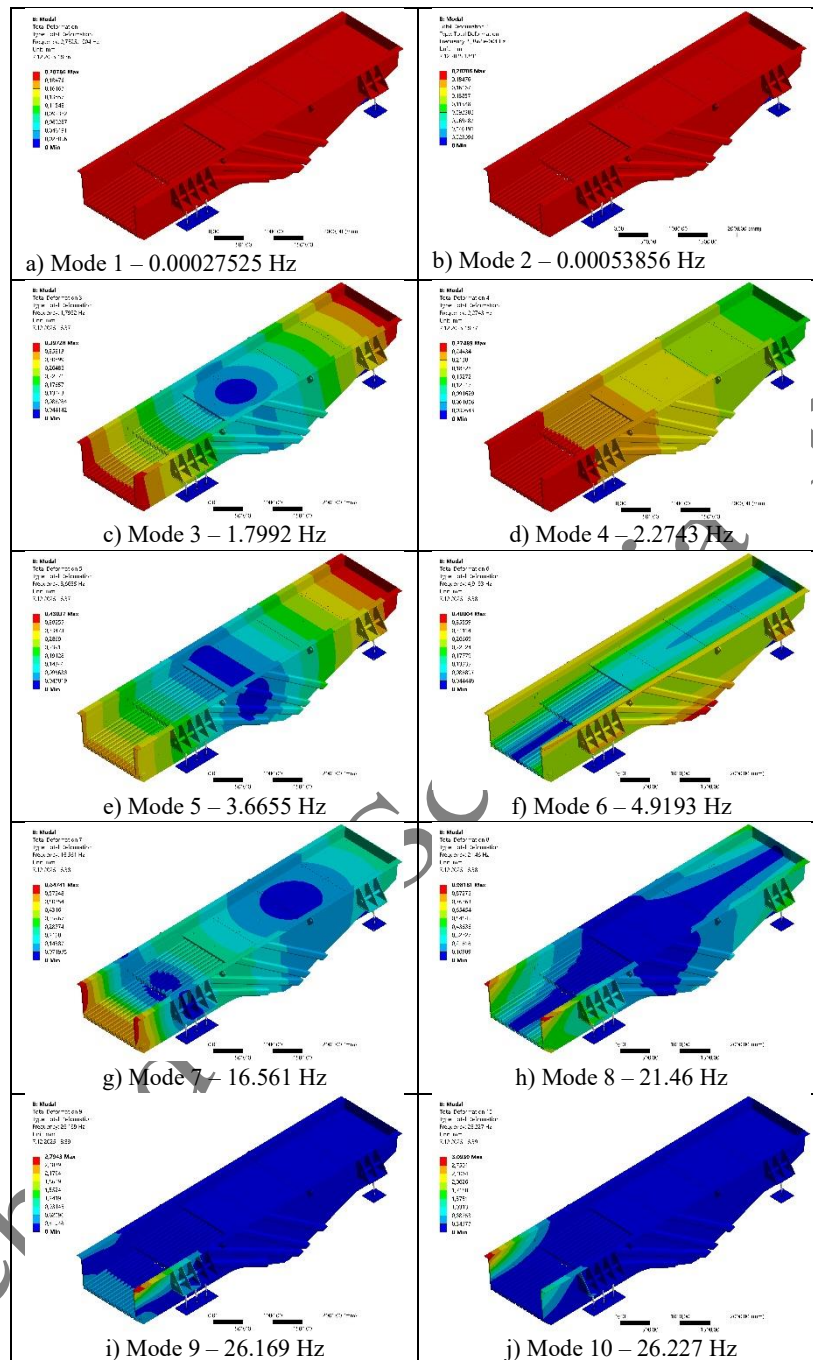


Table 5. List of ratio of effective mass to total mass

Mode No.	X Direction	Y Direction	Z Direction
1	3.87E-01	0.98856	6.13E-15
2	0.98856	3.87E-01	6.18E-14
3	2.09E-12	8.58E-12	1.98E-01
4	7.16E-14	3.88E-15	0.95785
5	2.20E-14	1.43E-15	3.07E+02
6	1.99E-16	4.13E-14	2.86E-03
7	1.22E-16	1.26E-15	5.90E-06
8	1.70E-19	6.79E-19	9.31E-05
9	4.46E-19	2.66E-16	2.26E-02
10	6.35E-18	2.02E-16	7.21E-02
Sum	0.9886	0.9886	0.9886

Table 6. Mass participation in X-, Y- and Z- directions for natural frequencies

Mode No	Frequency (Hz)	Effective Mass (kg)		
		in X-Direction	in Y-Direction	in Z-Direction
1	0.0003	0.9	23,101.7	1.43E-10
2	0.0005	23,101.7	0.9	1.44E-09
3	1.7992	4.88E-08	2.00E-07	4,617.5
4	2.2743	1.67E-09	9.06E-11	22,384.0
5	3.6655	5.15E-10	3.33E-11	7.2
6	4.9193	4.64E-12	9.64E-10	66.8
7	16.5610	2.84E-12	2.95E-11	0.1
8	21.4600	3.98E-15	1.59E-14	2.2
9	26.1690	1.04E-14	6.21E-12	527.8
10	26.2270	1.48E-13	4.72E-12	1,685.9